ANNUAL REVIEWS

Annual Review of Astronomy and Astrophysics

Carrington Events

Hugh S. Hudson[1,2]

[1]School of Physics & Astronomy, University of Glasgow G12 8QQ, United Kingdom; email: hugh.hudson@glasgow.ac.uk

[2]Space Sciences Laboratory, University of California, Berkeley, California 94720, USA

Keywords

extreme events, flares, plasma physics, stellar magnetic activity, multimessenger astronomy, space weather

Abstract

The Carrington event in 1859, a solar flare with an associated geomagnetic storm, has served as a prototype of possible superflare occurrence on the Sun. Recent geophysical (^{14}C signatures in tree rings) and precise time-series photometry [the bolometric total solar irradiance (TSI) for the Sun, and the broadband photometry from *Kepler* and *Transiting Exoplanet Survey Satellite*, for the stars] have broadened our perspective on extreme events and the threats that they pose for Earth and for Earth-like exoplanets. This review assesses the mutual solar and/or stellar lessons learned and the status of our theoretical understanding of the new data, both stellar and solar, as they relate to the physics of the Carrington event. The discussion includes the event's implied coronal mass ejection, its potential "solar cosmic ray" production, and the observed geomagnetic disturbances based on the multimessenger information already available in that era. Taking the Carrington event as an exemplar of the most extreme solar event, and in the context of our rich modern knowledge of solar flare and/or coronal mass ejection events, we discuss the aspects of these processes that might be relevant to activity on solar-type stars, and in particular their superflares.

■ The Carrington flare of 1859, though powerful, did not significantly exceed the magnitudes of the greatest events observed in the modern era.
■ Stellar "superflare" events on solar-type stars may share common paradigms, and also suggest the possibility of a more extreme solar event at some time in the future.
■ We benefit from comparing the better-known microphysics of solar flares and coronal mass ejections with the diversity of related stellar phenomena.

Contents

1. INTRODUCTION

Technical and astronomical developments in the nineteenth century enabled many discoveries about solar magnetic activity. The early discoveries of sunspots and faculae in the seventeenth century eventually led to the observation of the Carrington flare in 1859 (Carrington 1859, Hodgson 1859): a chance occurrence just at the time of Carrington's careful and systematic daily recording of a particularly large sunspot group. As a bonus, a newly installed "self-recording magnetograph" documented some remarkable and apparently associated geomagnetic activity (Stewart 1860, 1861). That these astonishing developments (the visual flare and the crochet in the terrestrial magnetic field) should have occurred in close coincidence must have seemed even more astonishing; the explanations for this had to await the discoveries of short-wavelength radiation and the existence of an ionosphere. The Carrington event thus dramatically helped to inaugurate what we now may think of as time-domain astronomy, multimessenger astronomy, and space weather all at the same time.

The Carrington event involved multimessenger links to physics on the Sun that deserve some special attention. Its effects added to the list of messengers already known (since 1722; Graham 1724). Other messengers have appeared in the meantime (Hudson & Svalgaard 2019) but not including the neutrino emissions from solar activity that Davis (1993) had speculated about; we do not expect detectable fluxes of neutrinos from flares despite their nuclear physics.

Carrington himself, an accomplished astronomer with broad interests, had a brief but brilliant career (Clark 2007, Cliver & Keer 2012). A visitor to the Royal Astronomical Society at Burlington House, London (for example), can immediately recognize his impact by noting the outsized volumes along the shelves of the *Monthly Notices* for two years during his productive period; Cliver

Crochet: a small hook-like excursion of the geomagnetic time-series trace

Figure 1

Carrington's sunspot sketch from the day of the flare. Figure reproduced from Prosser (2018); copyright 2018 Oxford University Press.

& Keer (2012, their figure 1) show such a library shelf. His interesting life contained some social drama as well as great science.

Our interest in this singular phenomenon at the present day has to do with its status as an extreme solar event, perhaps as powerful as the Sun can provide or perhaps a clue toward the occurrence of similar even greater events at some time in the future. Danger lurks for humanity's technological assets, especially those in space, via the newly recognized space weather aspects of solar magnetic activity. The present moment finds us some fifty years into the space age, with burgeoning astronomical capabilities for studying flare phenomena in the stellar perspective, and this review aims to assess our knowledge of the likely physics of the Carrington event as a guide for the future. Schaefer et al. (2000) had suggested that extreme events (superflares) might actually occur on solar-type stars, and the *Kepler* photometric data gave that idea greater urgency; earlier speculation by Wdowczyk & Wolfendale (1977) had even considered a link between solar particles and ancient catastrophes on Earth. Such a huge flare can generally impact Earth and the human environment in three major ways: electromagnetic radiation (the flare), particle radiation (solar energetic particles or SEPs), and the impact of ejecta [coronal mass ejection (CME) and/or interplanetary coronal mass ejection (ICME) phenomena]. These general processes could also affect biology, if any, on an exoplanet whose star produced extreme events [see Cranmer (2017) for a recent theoretical overview of stellar CME physics].

Carrington had observed a white-light flare defined as one detected through a broad-band filter (in Carrington's case, by observation of a projection screen of a solar image with an 11-inch diameter). His actual sketch of the Sun from the day of the flare (Prosser 2018), shown in the color of his screen ("a pale distemper of straw"), appears in **Figure 1**. The recently adopted International Astronomical Union nomenclature describes the Carrington event as SOL1859-09-01T11:18, with the time field here referring to the event onset in Greenwich Mean Time (with typical care, Carrington set an uncertainty of 15 s on this time).

This review begins with a discussion of the Carrington event itself (Section 2), for which we have some direct and also some multimessenger information. Section 3 then gives a brief

Superflares: flare events with energy $>10^{33}$ erg

SEP: solar energetic particle

CME: coronal mass ejection

ICME: interplanetary coronal mass ejection

White-light flare: a flare, such as Carrington's, detected in a broad visual passband

overview of solar flare and/or CME knowledge, emphasizing the observational basis (e.g., Fletcher et al. 2011) but not hesitating to comment on theoretical problems as the author sees them; a knowledgeable reader can skip this section entirely. The anticipation of a solar extreme event, and the hints about this gained from stellar superflares (Schaefer et al. 2000), motivate a description of the new superflare observational material in Section 4. This consists of the probably-solar ^{14}C events found in tree-ring samples by Miyake et al. (2012, 2013) and the systematic observations of stellar activity via the sensitive *Kepler* photometry (Koch et al. 2010), especially the common occurrence of superflares on solar-type stars (Maehara et al. 2012). These discoveries have awakened an interest in the extreme events (e.g., Love 2012, Riley 2012) that may occur at any energy, given the distribution of flare energies as a power law (Section 5.3) with an indeterminate upper limit (Hudson 1991, Aschwanden 2019). Section 5 tries to fit the new facts into the solar (space weather, or terrestrial habitability) and stellar (exoplanet habitability) frameworks.

2. THE CARRINGTON FLARE ITSELF

2.1. Visual Sighting

The Carrington event happened, coincidentally, just as Carrington had conducted precise timing (positional) measurements of a great sunspot group. This keen observer's clear description and the accompanying sketch (**Figure 2**) described two bright patches that appeared to move at about 70 km s^{-1} during their 5-min period of visibility (see the sidebar titled The Radiant Energy of the Carrington Flare). By good fortune, his friend Hodgson—at a separate observatory—also saw the event but without resolving it into two components. He did make a useful statement about the flare's color and brightness, comparing it with how α Lyr would appear, as seen in a "large telescope with low power" (Hodgson 1859, p. 16).

These descriptions do not disagree with the appearance of white-light flares (Section 3.2.2) in the modern era, and we can use them to derive a crude estimate of the total radiated energy of the event (e.g., Neidig 1989, Hudson 2016). This estimate, considering the discussion in Section 3.2.4,
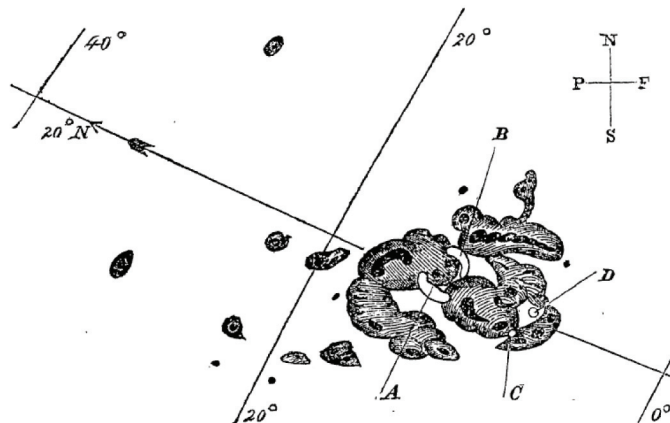
Figure 2

Carrington's sketch of the 1859 flare: four regions of brightening (*A* and *B* at the beginning, *C* and *D* 5 min later) in the midst of a major sunspot group. *P* and *F* denote preceding and following in the sense of solar rotation. The *N* and *S* are geographic. Figure reproduced from Carrington (1859); copyright 1859 Oxford University Press.

THE RADIANT ENERGY OF THE CARRINGTON FLARE

An estimate of the total radiated energy of the Carrington flare at 4×10^{32} erg, based on his careful sketch and description, does not exceed that of more recent flares. Assuming a mass of 10^{16} g, the CME had a kinetic energy of about 3×10^{32} erg.

can help us place the event in the context of flare occurrence statistics (Section 5.3). Inferring a flare spatial scale of 25 arcsec from Carrington's sketch, his reported duration of 300 s, and emission temperature of 10^4 K inspired by the α Lyr color comparison,[1] and a blackbody spectrum, one obtains 4×10^{32} erg for the total radiated energy. This easily derived number did not seem to make too much of an impression on colleagues at the time (the blackbody spectrum still lay in the future), but it does immediately place the Carrington event near the top of the (solar) flare energy list as known from the recent era. This, one could say, follows immediately from the event's nature as a major white-light flare.

The sunspot group in which the Carrington flare appeared (**Figures 1** and **2**) had an area comparable with that of the largest ever recorded. Aulanier et al. (2013), working with this sketch, described the group area as smaller than 6,000 MSH (millionths of solar hemisphere), although Newton (1943) quotes an area of only 2,300 MSH. Newton (1955) remarked that the greatest sunspot group area on record then was the 6,132 MSH (roughly 2% of the disk) estimated for a group in 1947. Since that time, many solar cycles in the past, no larger sunspot group seems to have appeared.

2.2. Geomagnetic Records

In the year prior to the Carrington event, a seemingly unrelated technological innovation had begun routine observation at the Kew Gardens Observatory: a sensitive instrument that photographically recorded the fluctuations in the geomagnetic field (Stewart 1860). The superintendent at Kew (Mr. John Welsh; Sabine 1871) had installed this self-recording magnetograph, which permitted high time resolution, with high sensitivity as well, and generated a durable record, all without the benefit of any electronics! Its recording provided the tracing shown here as **Figure 3**.

The first striking feature of the magnetometer record is the crochet[2] at the time of the flare (shown as 11:15 GMT, which is consistent within uncertainties to Carrington's more exactly recorded onset time for the visual flare). Some 18 h later, the initial deflection (storm sudden commencement) signaling the beginning of a major geomagnetic storm appeared. In hindsight, we realize that the flare had emitted ionizing radiation that instantaneously enabled a new current system to flow in Earth's ionosphere (Dellinger 1936), producing the crochet, marking the initiation of an ICME that transported a massive plasma cloud across the heliosphere. This would have impacted the magnetosphere and driven the ensuing magnetic storm. The shock wave preceding the ICME caused the storm sudden commencement. Comparison of the Carrington solar flare effect (SFE) with a modern event, SOL2003-11-04 (Cliver & Dietrich 2013, Curto 2020),
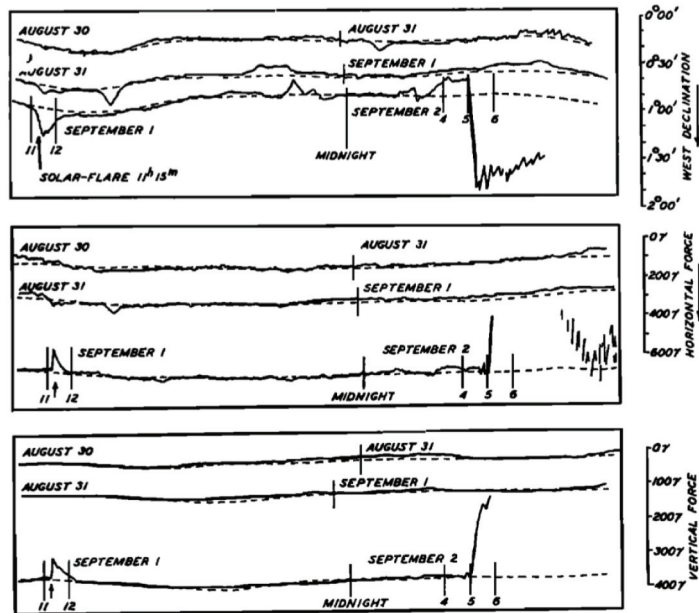
Millionths of solar hemisphere (MSH): a measurement of sunspot area

SFE: solar flare effect; same as crochet

---

[1] A brilliant anticipation; see Kowalski et al. (2010).
[2] Originally spelled crotchet, designating a hook-like glitch in the magnetometer signal (Newton 1943). This type of ionospheric disturbance is more prosaically known now as an SFE.

Figure 3

The Kew magnetometer records, as reduced by Bartels (1937). Each panel shows one vector component of the terrestrial magnetic field, and in each panel three lines show consecutive daily traces. The "crochet" on September 1 and the geomagnetic storm onset on September 2 show up strikingly by comparison with the two preceding quiet days. The units of the measurements here are angle for the compass declination, and $\gamma = 10^{-5}$ G for the "force" (magnetic intensity) in the vertical and horizontal projections. Figure reproduced from Bartels (1937); copyright 1937 Oxford University Press.

suggests that both flare events had effective GOES (*Geostationary Orbiting Environmental Satellite*) classifications[3] of about X45. The ionospheric effects in an SFE appear to have comparable contributions from soft X-rays and from Lyman-α flare emissions (Curto et al. 2016).

The term geoeffectiveness describes the many effects a flare and/or CME can have on the terrestrial environment. This includes the magnetic storm but also the many other complicated processes, nowadays including the SEP radiation storm outside the magnetosphere itself. The strength of the magnetic storm, for example, depends upon both the heliographic coordinates of the solar event and the orientation of the magnetic field in the ejecta (ICME) in relation to the geomagnetic field. These conditions all fortuitously came together for the Carrington event. One should note historically that the lack of a one-to-one matching of solar and terrestrial effects convinced many in the nineteenth century that the Carrington event's remarkable geomagnetic consequences might have been merely a coincidence; none of the other nineteenth-century flare events mentioned below seem to have had similar geoeffectiveness (Nevanlinna 2006).

This explanation involves several concepts unknown in 1859 and still in the process of refinement at present; for example, **Figure 4** shows a modern example of a crochet: In this, via the timing match, one sees that flare-emitted Lyman-α radiation plays a role (Milligan et al. 2020).

---

[3]The GOES soft X-ray irradiances are traditionally described in logarithmic ranges of ABCMX, where Xn means $n \times 10^{-4}$ W m^{-2} in the standard 1–8-Å band.
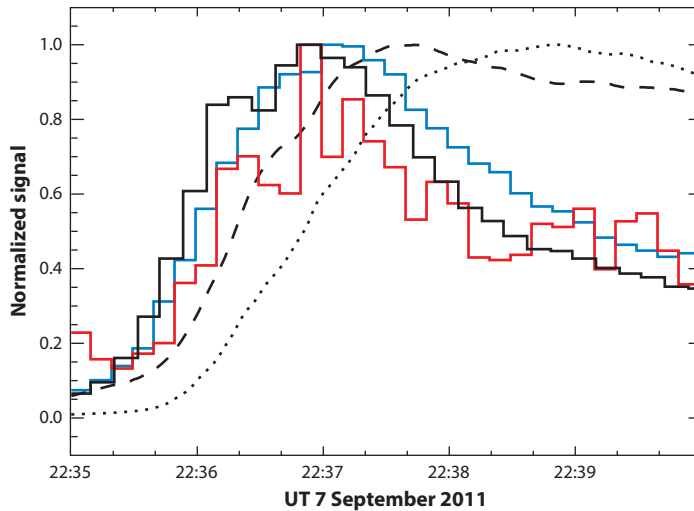
Figure 4

A recent SFE (*dashed black line*) illustrating the prompt ionospheric response to various flare radiations. This is a modern geomagnetic crochet, as seen for the Carrington event in **Figure 3**, observed here by the Kakioka Geomagnetic Observatory (Japan). Solar Lyman-α radiation and other EUV emissions coincident with the flare impulsive phase suddenly increase the ionization in the ionospheric E-region, leading to the current system affecting the ground-based magnetometer. Here, we show the impulsive phase via time series of EVE He II 304 Å (in *blue*) and Fe X 171 Å (in *red*), and GOES Lyman-α (*black histogram*). The SFE peak is delayed from the impulsive phase, but clearly precedes the GOES 1–8-Å coronal X-ray maximum at 22:38 UT (*dotted line*). Abbreviations: EUV, extreme ultraviolet; EVE, EUV Variability Experiment; GOES, *Geostationary Orbiting Environmental Satellite*; SFE, solar flare effect.

This is significant for flare physics because it helps to define the impulsive phase, as discussed below in Section 3.

2.3. Other Nineteenth-Century Solar Flares

The Carrington event did not inspire a flood of new observations of solar flares. The basic problem lay in the lack of the sensitive observables, such as Hα and soft X-rays, introduced over the subsequent decades. To the author's knowledge, only five solar flares were detected in the nineteenth century in white light, including the Carrington event itself: four described by Švestka (1976) and a fifth recently rediscovered by Vaquero et al. (2017). **Table 1** lists them all. Other nineteenth-century flares were detected spectroscopically as Hα line reversals (e.g., Newton 1943) but not reported in the continuum.

Table 1   White-light solar flares observed in the nineteenth century

Observer	Flare	Reference
Carrington	SOL1859-09-01	Carrington 1859
Secchi	SOL1872-11-13	Secchi 1872
Valderrama	SOL1886-09-10	Valderrama 1886, Vaquero et al. 2017
Trouvelot	SOL1891-06-17	Trouvelot 1891
Rudaux	SOL1892-07-15	Rudaux 1892

Each of these cases must have come via a chance opportunity seized by an observer as keen as Carrington, and we may suppose that other examples must have occurred but then were dismissed as not credible. The published data for these additional early events do not suffice to make the simple estimates done for the Carrington event (Section 2); thus, we do not attempt to compare event magnitudes, but as white-light flares they automatically rank among the most energetic. What seems clear from the lack of fuss is that the nineteenth-century observers failed to get flare physics into the mainstream of astrophysics even for the phenomenon itself, much less for the geomagnetic connection and space weather, which (though compelling in 1859) seemed nonreproducible and therefore of questionable validity.

2.4. What Is a Carrington Event?

The discussion above does not suggest anything unusual about the Carrington flare itself, except for possibly its magnitude (to be discussed in that context in Section 5.3 below). Nevertheless, we adopt it as the prototype extreme event, justified by its situation among at most a few others at the maximum end of the power-law distribution of event occurrence, and therefore it hints at still greater events occurring over longer timescales. In particular, the visual estimate from Carrington's own data and the instantaneous ionospheric effects reported by ground-based magnetometers (the SFE or crochet) both point to similar magnitudes for the Carrington flare and for other more recent major events, such as SOL2003-11-04 (discussed further in Section 5.4). In the following, we review our knowledge of extreme solar events from the point of view of their physics and in the context of the still more energetic events known to occur on more active stars.

This review emphasizes the solar and/or stellar astronomical inferences from the Carrington flare, namely its association with an extreme geomagnetic storm and the impetus it gave to modern interest in space weather (see, e.g., Tsurutani et al. 2003, Cliver & Svalgaard 2004, Schrijver et al. 2012, Hayakawa et al. 2019). The disturbances included interruptions of telegraph services (with fires in telegraph offices; Boteler 2006) and aurorae in the tropics (Shea & Smart 2006).

3. SOLAR FLARES AND CORONAL MASS EJECTIONS

3.1. General Considerations

In this lengthy section, we give an overview of our current understanding of flare and/or CME physics as a guide to the possibilities for solar superflare occurrence. Solar flares and CMEs, both extremely well-studied, represent the two most obvious manifestations of magnetic activity in the solar atmosphere. Ultimately, the consensus holds that these major events, plus a host of lesser phenomena of perhaps comparable violence, arise from magnetic flux emergence. This term defines the observational environment for the development of coronal magnetic structure and its charging with energy and helicity. Dynamo action in the interior produces organized magnetic fields that penetrate the photosphere and then spread throughout the solar atmosphere, containing stresses due to embedded current systems. The field in the low corona typically has plasma β well below unity, and thus the magnetism defines the atmospheric structure of the corona and innermost heliosphere. The physics of flux emergence involves the transport of energy via the Poynting vector, as well as the twisted nature of the field describable as helicity or as field-aligned currents. See e.g., van Driel-Gesztelyi & Green (2015) and Toriumi & Wang (2019) for recent reviews of solar active regions and their behavior.

Both flares (e.g., Fletcher et al. 2011) and CMEs (e.g., Chen 2011), which often go together, result from the sudden extraction of magnetic free energy on short timescales and its distribution into other forms. This requires the operation of plasma instabilities and the restructuring of the coronal magnetic field, usually described in terms of magnetic reconnection or flux transfer. An
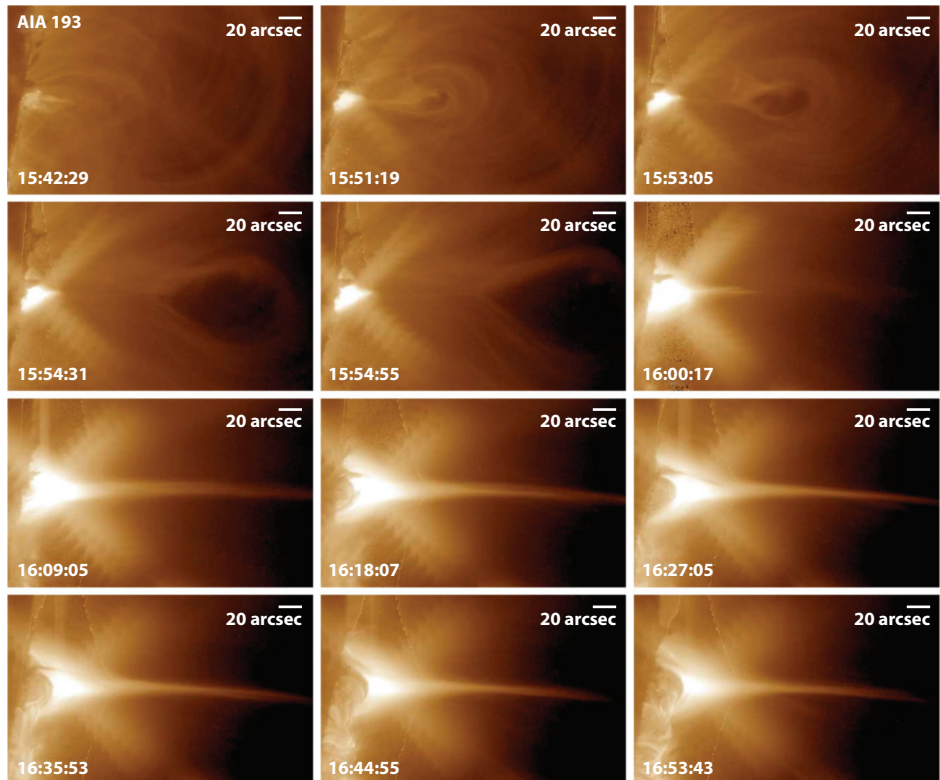
energy release may or may not result in an eruption of the field as the observable mass motion of a CME; if not, the result is simply enhanced radiation across an extremely wide spectral range, and the disturbance is purely a flare. If an eruption of the field occurs, a large amount of the released magnetic energy may go into the CME kinetic energy and eventually even into high-energy particles (e.g., Hudson & Ryan 1995). The details of the partitioning of the energy release remain somewhat ill-defined because of observational unknowns as well as theoretical weaknesses (e.g., Emslie et al. 2012, Aschwanden et al. 2017). Again, one should remember that these events often involve plasmas at $\beta \ll 1$, meaning that the dynamically important structures may not be readily visible at any wavelength—the emissions may help us to understand these structures but may not directly represent the important components. These disruptions ultimately derive their energy and momentum (e.g., Hudson 2011) solely from the star's dynamics (convection, rotation, and oscillation).

We can use the Carrington event as a prototype of a flare and/or CME disruption that can occur in the magnetized atmosphere of a solitary star even if we do not have the full set of modern data. The recent flare SOL2017-09-10, illustrated in **Figure 5**, probably has a close resemblance to what the Carrington flare would have looked like with modern instrumentation (e.g., Warren et al. 2018) if observed at the limb in a perspective almost parallel to the model's current sheet. The current sheet is a key feature of the CSHKP (Carmichael–Sturrock–Hirayama–Kopp & Pneuman) model described in Section 3.2.3 below.

Globally, we can distinguish two other distinct electrodynamic environments for flare-like disruptions (see the sidebar titled Electrodynamic Environments): A planetary atmosphere embedded in a stellar wind necessarily experiences a convective electric field from the flow, leading to the paradigm of the Dungey cycle of magnetic reconnection in the magnetopause and in the magnetic tail (recounted by Dungey 1994) in a rich and interesting history involving Giovanelli, Hoyle, Cowling, and Sturrock, among others. Solar flares and magnetospheric substorms notoriously have points of similarity (e.g., Obayashi 1975, Bratenahl & Baum 1976). However, the external driver provided by the solar-wind flow around the magnetospheric cavity of course does not exist on the Sun. Another major point of difference is the electrical neutrality of Earth's atmosphere. In the case of binary stars and accretion disks, an external supply of mass and energy can drive the electrodynamic phenomena, as in the store-and-dump periodic behavior of the rapid burster (Lewin et al. 1967), an early discovery in X-ray astronomy. Again, these resources do not help us understand the build-up and release behavior of magnetic energy release in the atmosphere of an isolated star such as the Sun, which remains essentially unexplained to this day (e.g., Gaizauskas & Švestka 1987).

The distinction between a flare and a CME may resemble a dynamic version of the distinction between the corona and the solar wind. A classical three-part CME involves plasma flows perpendicular to the field direction, with the appearance of rising loops, and these motions increase the open magnetic field locally (Lockwood 2013). Here, an open field connects the photosphere with the heliosphere, as defined (for example) by the place where the bulk flow of the solar wind exceeds the local sound speed. Interestingly, this often-repeated eruption process, sometimes involving several CMEs per day with each one appearing to open a large fraction (perhaps as much as 10%) of the total magnetic flux at the coronal base, results in only a weak solar-cycle dependence of the fraction of open magnetic field (e.g., Lockwood 2013). The presence or absence of a CME in a given solar event obviously has a major impact on its geoeffectiveness, because the impact of the solar ejecta on the magnetosphere produces the delayed effect such as that visible in **Figure 3** for the Carrington event.

Much of solar research on flares and CMEs explores spatially resolved detail, with multimessenger access to particles and fields measured in situ rather than by astronomical techniques.

Carmichael–Sturrock–Hirayama–Kopp & Pneuman model (CSHKP): a flare model involving an erupting bipolar field and subsequent magnetic reconnection

Figure 5

The remarkable flare/CME event SOL2017-09-10, which embodies many of the features that we think nineteenth-century technology missed in the Carrington event: (*upper left* to *lower right*) a 70-min development sequence of this typical recent CSHKP flare. This limb view of such an event reveals features actually not detectable even in this era for an on-disk event, such as Carrington's. As seen in the AIA 193-Å EUV band, the eruption begins in a compact region just at the W limb of the Sun (just visible as a dark edge at the *left*). It continues with a rising (to the *right*) plasmoid, seen best in the top-row frames; a bright thin structure identified as a plasma sheet enveloping a true current sheet, but still quite thin; and a substantial widespread dimming (compare the *first* and *last frames*; we interpret this kind of dimming simply as the CME mass loss; Hudson & Webb 1997). The diagonal features at ±45 deg diagonal are instrumental diffraction artifacts caused by the bright loop-top/cusp sources. Figure adapted with permission from Warren et al. (2018); copyright 2018 AAS. Abbreviations: CME, coronal mass ejection; CSHKP, Carmichael–Sturrock–Hirayama–Kopp & Pneuman; EUV, extreme ultraviolet. The image presumably shows a thick, hot (some 20 MK at its base) plasma sheet surrounding the mathematically singular current sheet required by the model.

Dimming: the sudden stepwise disappearance of a coronal volume

Stellar observations do not have these advantages. Flares greatly outnumber CMEs, so the in situ messengers may not always arrive. Strikingly, though, the CME component of a composite solar event not only happens but also may sometimes dominate over the flare component. Now often termed stealth CMEs (Robbrecht et al. 2009), some large-scale diffuse events may have almost no detectable low-corona or chromospheric counterpart (cf. Cliver et al. 2019). Theoretically a completely detached CME would make no physical sense, because ideally all of the heliospheric field must link to its sources in the surface of the Sun, even though in 2D cartoon representations an ejection may appear to be fully unlinked. Observations of transient coronal holes, i.e., long-lasting dimming regions, clearly establish this (Kahler & Hudson 2001). Intermediate cases, with

only weak low-coronal signatures (Harvey et al. 1986), also include the "*disparitions brusques*", in which (from one day to the next) a massive solar filament simply disappears. An early clear example (Olivieri 1948), shown here in **Figure 6**, makes it obvious retrospectively that the huge invisible magnetic structure required to support the long filament—with a size of order $R_\odot$, which is much larger than the scale of the supergranulation—has catastrophically changed overnight.

3.2. Models

In relating solar experience to stellar observations, it seems natural to wish to transfer a successful model of a solar flare or CME into the new environment. We currently do not have a predictive theory for the solar flare and/or CME events, but we do have descriptive paradigms that capture a great deal of the phenomenology: the simple loop, the thick-target model, and CSHKP. This section briefly describes these currently popular models for the solar phenomena, and ends with comments about their global properties, especially in the context of analogous stellar events.

3.2.1. The simple loop.
Soft X-ray and extreme ultraviolet (EUV) images of solar flares distinctly appear to consist of one, or usually multiple, magnetic loops. Accordingly, the simplest descriptive model consists of one of these building blocks, for which the Rosner–Tucker–Vaiana (RTV) scaling law (Rosner et al. 1978, Vesecky et al. 1979) provides an analytic lead-in: for a constant energy input into a steady-state compact loop, $T_{\max} \approx 1.4 \times 10^3 \, (pL)^{1/3}$ K, in terms of looptop temperature $T_{\max}$ (K), loop pressure p (dyne cm^{-2}), and loop spatial scale L (cm). This describes an equilibrium situation in the presence of an assumed and constant volumetric heat input, but the X-ray images of the crucial coronal regions of solar flares, notably with the *Skylab* telescopes (e.g., Sturrock 1980), revealed them also to consist of just such loop-like structures. These transient overpressure loops may not follow the RTV scaling. This has led to considerable theoretical and modeling work on the dynamical development of coronal loops, heated impulsively and creating high-pressure structures in the corona; a bright flare loop can have a gas pressure exceeding 10^3 dyne cm^{-2} (e.g., Reale 2014, Jejčič et al. 2018). These structures require strong magnetic fields (up to 1 kG for reasonable parameters) to contain them; we envision a low-β plasma in which the visible loops have somewhat lower magnetic pressures than the confining field and must resemble

EUV: extreme ultraviolet

Rosner–Tucker–Vaiana (RTV): scaling law relating physical parameters in a solar magnetic flux tube
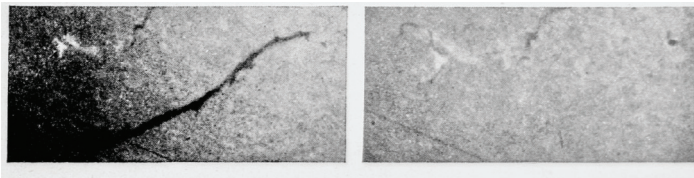
Figure 6

An early "stealth CME"? The two frames show the *"disparition brusque"* SOL1948-10-07, comparing images taken about 24 h apart. Figure reproduced from Olivieri (1948); copyright 1948 Société astronomique de France – Magazine L'astronomie. **https://saf-astronomie.fr/**.

coronal magnetic tunnels. Further analytic work on flare loops, describing them as they evolve, led to the full description by Cargill et al. (1995) and to the approximate but convenient numerical EBTEL ("enthalpy-based thermal evolution of loops model"; Klimchuck et al. 2008).

3.2.2. The thick target.

Thick target refers to a laboratory X-ray machine in which the radiating electron beam stops completely in the anode, integrating the bremsstrahlung emission from the electrons as they slow down collisionally. Alternatively, in a thin target X-ray machine, the electrons radiate as they pass through a thin foil and, thus, remain essentially monoenergetic.

Based upon the discovery of hard X-ray emission at the beginning of a solar flare (Peterson & Winckler 1958) and its interpretation as nonthermal bremsstrahlung continuum from mildly relativistic electrons (Anderson & Winckler 1962), one could identify the loop heating as owing to the collisional losses of electrons injected by some unknown mechanism operating in the corona. From a coronal electron source, known to exist via the radio type III (fast drift) emission (e.g., Wild et al. 1963), one could imagine a thick-target region in the dense chromosphere for electrons projected downward, rather than upward as in a type III burst. The existence of the rare reverse-slope type III emission (Tarnstrom & Zehntner 1975) lends some support for this idea. This kind of model matches the idea of the Neupert effect (Neupert 1968), but one should note that this very common morphology would result from any impulsive heating mechanism. The hard X-ray continuum and the microwave gyrosynchrotron radiation tend to occur at the beginning of a flare (the impulsive phase). The Neupert effect neatly allows one to think of the coronal soft X-ray sources and chromospheric line emissions (Hα) as showing the drastic evolution and heating of cool chromospheric mass injected (by evaporation) into coronal magnetic traps, where its soft X-ray emission constitutes the gradual phase of the flare.

The significance of hard X-ray emission resulted from the relatively small cross-section for the bremsstrahlung emission mechanism of nonrelativistic electrons; it is only 10^{-5}–10^{-4} as large as the Coulomb collisional cross-section, implying huge energy content in the electron beam (e.g., Brown 1971, Kane & Donnelly 1971). Furthermore, this toy model also implies a correspondingly huge electric current within the beam, which must drive a return current (e.g., van den Oord 1990) for which the theory remains incomplete (e.g., Melrose 2017). The return-current problem has a close relationship with the number problem: The beam intensity required by thick-target modeling can imply that the coronal flux tube must accelerate more electrons than it could have held prior to the flare (e.g., Fletcher & Hudson 2008).

As with the static RTV loop, one can explore the parameter space of an essentially 1D forward model: the heating and cooling of a loop anchored in the chromosphere and extending into the corona, nominally assumed to have symmetric anchors (footpoints) embedded (line-tied) in a rigid chromosphere in opposite-polarity regions. Numerical modeling in the framework of radiation hydrodynamics, introduced by Nagai (1980), continues actively with the RADYN model of Carlsson & Stein (1997) and the HYDRAD model of Bradshaw & Mason (2003), among others. In this kind of modeling, one envisions the energization of electrons in the corona and their precipitation into the lower atmosphere along a 1D trajectory. The great advantage of such models lies in their ability to address radiative-transfer issues, at least in 1D, and to enable calculation of observables such as spectral line profiles and continua. Kowalski et al. (2015) have used such a model for dMe stellar flares, finding that they could reproduce the remarkable spectroscopic observations of Kowalski et al. (2010): The flare spectrum suggested the sudden appearance of a miniature A0-star photosphere in the flaring atmosphere of the dMe flare star YZ Canis Minoris (**Figure 7**). The implied temperature of about 10^4 K suggests regulation by hydrogen ionization.

McCracken (1959) had noted that solar cosmic rays (now termed SEPs) tended strongly to associate with white-light flares, of which the Carrington flare gave us the first example. This
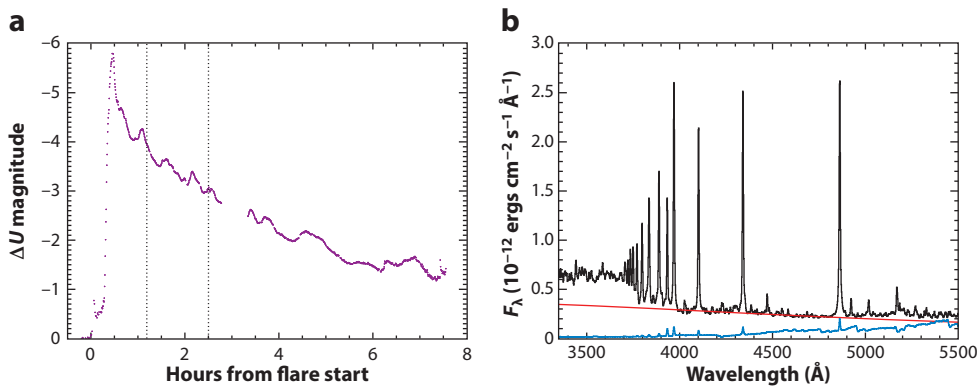
Figure 7

Time series (*a*) and optical–UV spectrum (*b*) for a megaflare on YZ CMi for the time interval indicated by dotted lines in panel *a*. The sharply defined Balmer series calls to mind an A0 star, even though the quiescent stellar spectrum (*blue lower trace*) shows no sign of this surprising phenomenon. The red line identifies the flare Paschen continuum. Figure adapted with permission from Kowalski et al. (2010); copyright 2010 AAS.

relationship suggested hard X-ray bremsstrahlung from precipitating electrons, or similarly γ-ray line emission from precipitation of protons, expected to be present in white-light flares because of their correlation with solar protons (Najita & Orrall 1970, Švestka 1970). Hudson (1972) also linked this thick-target action with white-light flare occurrence.

3.2.3. The Carmichael–Sturrock–Hirayama–Kopp & Pneuman model.

The prevailing paradigm for eruptive solar flares did not come from this SEP association, however, but rather from the behavior of Hα loop prominence systems, large structures that appeared well after the beginning of the event (Dodson 1961, Bruzek 1964). Even at this early date these structures had a clear association with hot and dense coronal volumes, quaintly termed sporadic coronal condensations, described in a series of papers by Jefferies & Orrall (1961, *et seq*). This theoretical work incorporated high-temperature plasmas and nonthermal particles within these volumes, visible in the Ca xv yellow coronal line. The *Skylab* soft X-ray observations of hot, dense loop systems confirmed this picture nicely: The hot plasmas form impulsively by chromospheric evaporation (the Neupert effect), and then gradually cool, eventually collapsing into Hα emission via the Field (1965) thermal instability. A major eruptive flare event does have a close association with the acceleration of SEPs, which is an important association for interpreting the radioisotope records (Section 4.2) and for exoplanet habitability.

By fits and starts, theorists began to concentrate on this behavior of eruptive flares, leading to the CSHKP picture (Carmichael 1964, Sturrock 1966, Hirayama 1974, Kopp & Pneuman 1976)[4] as summarized by Moore et al. (2001) and Shibata & Magara (2011), for example. In this scenario, the erupting solar magnetic field pushes coronal material out into the heliosphere as a CME, leaving a current sheet behind (a 2D manifold), as well as a flare arcade of hot X-ray-emitting loops that result when magnetic reconnection restores the closed field, leading eventually to the Hα loop prominence system. A 3D version of this model can incorporate a flux rope (e.g., Janvier et al. 2013), either formed during the eruption or perhaps preexisting as a part of the structure

**Loop prominence systems:** arcades of loops observed in Hα late in the flare development

Chromospheric evaporation: the heating and ablation of cool chromospheric plasma to create coronal X-ray sources

---

[4]Sadly, this name misses the initials of many other major contributors: Giovanelli (1946), Bratenahl & Baum (1976), Heyvaerts et al. (1977), Syrovatskii (1981), etc., to name only a few.
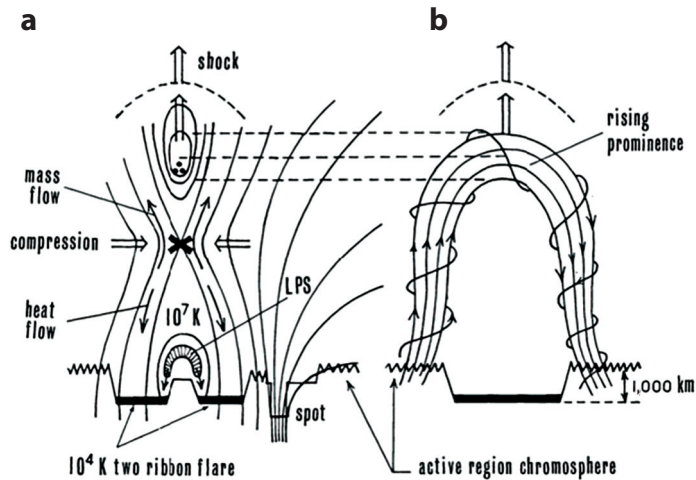
Figure 8

Two views of an early representation of the essence of the CSHKP flare model (the "H" is Hirayama 1974):
A sheared bipolar field entraining a filament erupts, and in its wake the stretched-out field lines
reconnect to produce the hot X-ray emitting loops, which cool to form the Hα loop prominence system.
Panel *a* shows the view along the filament channel/eventual loop arcade, as seen in **Figure 5**, with
panel *b* perpendicular to that axis. The elongated erupting filament channel naturally evolves into a basically
cylindrical arcade of loops, rooted in roughly parallel ribbons of Hα flare emission. Initially closed
field lines have become open in this process. (See Welsch 2018 for a recent theoretical analysis.)
Figure adapted with permission from Hirayama (1974); copyright 1974 Springer Nature B.V.
Abbreviations: CSHKP, Carmichael–Sturrock–Hirayama–Kopp & Pneuman; LPS, loop prominence system.

supporting the filament; in situ observations can detect this flux rope as a magnetic cloud (Burlaga
et al. 1982) as it rises through the heliosphere.

   Figure 8 (Hirayama 1974) had captured the essential geometrical features of CSHKP already;
subsequent developments have not actually added much to this picture, but magnetohydrody-
namic (MHD) simulations can follow its development so successfully that the geometry is quite
certain. Note that this early schematic not only makes the link between flaring and filament erup-
tion, which characterizes most of the really powerful flare and/or CME events, but it also clearly
describes the overpressure in the flaring loop footpoints. This moves the transition region (bottom
of corona) physically downward to allow for hydrostatic forces. This perceptive sketch does miss
the current-sheet nature of the reconnection region, though this turns out to dominate the actual
coronal geometry. The schematic, simple though it seems, really does anticipate events such as
that shown in **Figure 5**, which was an event occurring almost on the line of cylindrical symmetry
in **Figure 8*b*.** The CSHKP model captures the geometry and the time development of that event
and, presumably therefore, the Carrington event as well.

3.2.4. The global properties of these events. These concepts each have inspired many
schematics cartoons,[5] which are useful for relating one observable to another and for illustrat-
ing physical processes such as Fermi acceleration and magnetic reconnection. In many cases,
these schematics simply try to capture the geometrical appearance of the phenomena as empirical

---

[5]The author maintains a full archive of flare and/or CME sketches at **http://www.astro.gla.ac.uk/cartoons/**
for those interested in this approach.

descriptions, but they often have backup in the form of powerful numerical simulations. The global properties of the flare and/or CME phenomenon include the conservation of energy and momentum, the effects of force balance, MHD properties and electrodynamics, etc., and must encompass the way a magnetized stellar atmosphere can become locally unstable.

Even at the global level, and even on the Sun, we have uncertainties about the basics: Starting with the simplest one, what is the total energy release in a given event? We can observe much of the spectrum of the radiation, but with big gaps in the IR and particularly the UV shortward of the Balmer edge, and our estimates of total flare energy have large uncertainties. Emslie et al. (2012) have most recently attempted to describe the energy partition of a major flare and/or CME event, covering all forms of energy in an effort to establish its distribution among radiation, kinetic energy of ejecta, gravitational potential energy, enthalpy, particle acceleration, and, of course, the source of it all: the magnetic energy. A CME in particular represents a puzzle for the total magnetic energy, because it manifestly opens a large fraction of the coronal magnetic field, with the appearance of increasing its energy via the logic of the Aly–Sturrock conjecture (Aly 1991, Sturrock 1991); Aly states that "any spontaneous transition of the coronal field to an open state is precluded" theoretically (Aly 1991, p. L61; cf. Hudson 2011). In contrast, large perturbations of the photospheric magnetic field do accompany major events (Wang et al. 1994, Sudol & Harvey 2005) and NLFF (nonlinear force-free field) magnetic modeling does suggest that these changes do result in reductions of the stored magnetic energy in some cases (e.g., Sun et al. 2012).

The substantial problem for the two standard flare and/or CME paradigms (loop and/or thick target and CSHKP) lies in their disjointedness. An MHD model does not incorporate particles (energetically decisive), and the 1D radiation hydrodynamics models do not incorporate magnetic structure (also energetically decisive): In the global sense, neither can therefore express simple energy conservation. We can report one piece of global progress, however. The Parker–Melrose debate (Melrose 1995, Parker 1996), about the neutralization of coronal currents—a critical factor for energy storage—has now resolved itself observationally in favor of appreciable nonneutralization (e.g., Georgoulis et al. 2012). This implies a theoretical need to consider DC currents, finite electrical potentials, ion-neutral coupling, and non-Maxwellian particle distribution functions in detail in the chromosphere and lower corona.

4. SUPERFLARE DISCOVERY

Two recent observational departures have reawakened our interest in extreme solar events and the Carrington event in general: the new systematic stellar photometry, especially from *Kepler* and *Transiting Exoplanet Survey Satellite* (TESS), and the remarkable tree-ring ^{14}C discoveries. We discuss the impacts of these new developments individually below. They both point to superflares, in a restricted sense, as referring to flares more powerful than the Carrington event. Stellar flares in this category frequently occur on classical dMe flare stars and in a wide range of other stellar situations, on solitary stars as well as binary systems, reaching up to the novae. Our chief interest here is with superflares on solar-type ones (slowly-rotating G dwarf solitary stars).

4.1. New Stellar Time-Series Photometry

Stellar time-series photometry has taken giant steps forward with the *Kepler* (Koch et al. 2010) and TESS (Ricker et al. 2015) missions. These report broad-band optical variations of medium and bright stars with great precision, and for huge catalogs of objects. As missions dedicated mainly to planet-finding, the data do not have any optimization for flare observations (long integrations; no spectral information), but even so the *Kepler* data immediately provided interesting observations of flares on a wide variety of stars (Walkowicz et al. 2011). The same problem applies to our
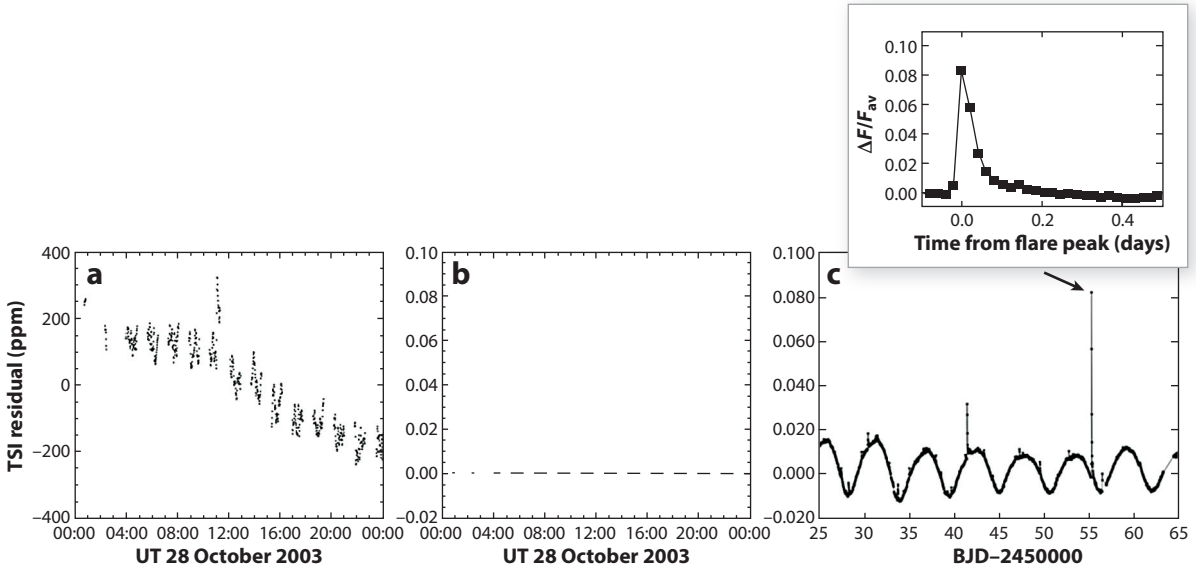
Figure 9

Solar and stellar bolometric flares, expressed as normalized residuals. (*a*) The best example of a solar flare detected in TSI monitoring from the SORCE/TIM experiment (Kopp et al. 2005), at a significance of about 5.5σ in 100-s sampling. (*b*) The same data on the abscissa scaling of panel *c*, a *Kepler* superflare time series shown on two timescales, as labeled. The solar time series shows low-level fluctuations due to convective flows and *p*-modes. The much larger and smoother variations in the stellar time series are presumably due to starspots of much greater scale and duration than sunspots. Panel *a* adapted from Woods et al. (2006). Panel *c* adapted with permission from Maehara et al. (2012); copyright 2012 Springer Nature B.V. Abbreviations: SORCE, *Solar Radiation and Climate Experiment*; TIM, Total Irradiance Monitor; TSI, total solar irradiance.

solar data, those dedicated to bolometric observations of the total solar irradiance (TSI, the solar constant); these precise data typically have sampling times of 2 min and therefore do not resolve important timescales. These extensive TSI data extend from 1981 to the present time, with several spacecraft contributing. Each of these aims at absolute photometry, but in practice they have not agreed mutually as well as they should have (see especially Kopp & Lean 2011). The basic solar TSI measurements also have no color information.

Figure 9 contrasts a maximal solar flare with stellar superflares. There are striking differences: Solar flares barely reach detectability, as limited by the broad-band fluctuations resulting mainly from convective flows in the photosphere and the *p*-modes. This continuum has a magnitude of about 4.4×10^{-6} Hz^{-1} at 100 µHz (Hudson & Woodard 1983, Hudson 1988) in the flicker noise domain (Bastien et al. 2013). The most significant detection (**Figure 9a**) shows SOL2003-10-28 at an estimated[6] total radiated energy of $(6 \pm 3) \times 10^{32}$ erg. These estimates roughly match those of Section 2 for the Carrington flare.

Note the utter contrast between these two variability patterns: the solar background variability has a broad-band nature, with an amplitude of order 50 ppm RMS on 2-min sampling; the *Kepler* star KIC 6034120 has a slow quasi-sinusoidal background variation measured in percentages, thus two orders of magnitude greater than the solar variation, due presumably to large, long-lived and

___

[6]Kopp et al. (2005); they also quote a total-energy estimate of $5(+4, -2) \times 10^{32}$ erg, and further give an estimate of 4.61×10^{32} erg for the same quantity, but with no uncertainty estimate.
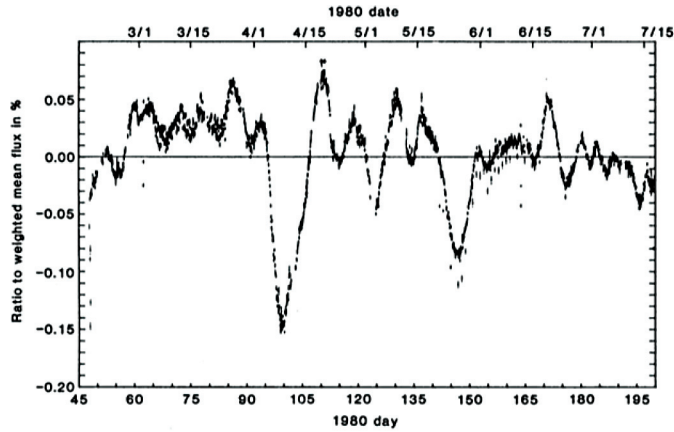
Figure 10

The first good total solar irradiance time-series observations from space (Willson et al. 1981), the rough equivalent of the *Kepler* photometry for the stars. One sees two "dips" due to independently occurring sunspot groups transiting the visible hemisphere around day numbers 99 and 146. This early data reduction has some flaws as published in 1981, but nicely reveals the broadband background fluctuations due to convective motions and *p*-mode oscillations, as described in the sidebar titled Flariness Versus Dippiness. Figure reproduced with permission from Willson et al. (1981).

stable star spot groups. These spots also differ strongly from solar spots because they have lifetimes greatly in excess of the rotation period. Furthermore, the star clearly shows flares, whereas the Sun does not; and finally, the Sun shows characteristic dips, whereas the star does not. **Figure 10** shows two of these dips in the first TSI observations from space; each one, lasting about 1/4 rotation period due to foreshortening, reflects the disk passage of a large sunspot group. The sunspots have lifetimes comparable with the rotation period and seldom repeat, making solar gyrochronology difficult at least during sunspot maximum periods. A *Kepler* solar-type star (Notsu et al. 2019) does not look at all like the Sun in these ways, presumably because of its age and/or its more rapid rotation. The *Kepler* flares are white-light flares in the sense of broad-band detection, roughly comparable with the solar TSI bolometric measurement (see the sidebar titled Flariness Versus Dippiness).

4.2. Solar Energetic Particles and the Radioisotope Record

Extreme events involve the copious acceleration of solar cosmic rays or SEPs (e.g., Desai & Giacalone 2016). These particles have a close relationship with the massive ejecta (up to 10^{16} g

FLARINESS VERSUS DIPPINESS

The solar TSI exhibits low-level (of order 50 ppm per 2-min sample) fluctuations due to *p*-mode oscillations and a broad-band flicker noise continuum with amplitude of about 4.4×10^{-6} Hz^{-1} at 100 μHz (Hudson & Woodard 1983), plus pronounced dips due to one-off sunspot transits—dippiness. Flares rarely and only marginally exceed these background fluctuations (**Figure 9**). The *Kepler* time series for most superflare stars do not show dips, but instead have persistent quasi-sinusoidal variability at large amplitude (percentages), plus the striking flare excesses—flariness.
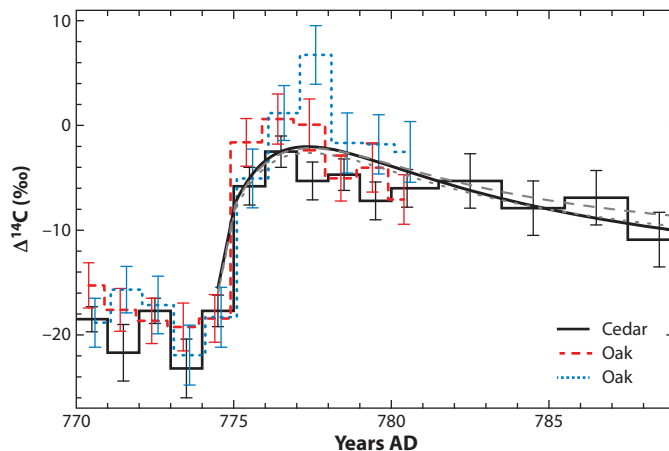
Figure 11

The circa 774 AD event, with European oak tree-ring data added to the Japanese cedar data, and with a model of the terrestrial carbon cycle overplotted (from Usoskin et al. 2013, who explain the $\Delta^{14}C$ measure in the context of the terrestrial carbon circulation). Figure adapted with permission from Miyake et al. (2012); copyright 2012 Springer Nature B.V.

per event) seen as CMEs in coronagraphs and spreading out into the heliosphere. The bow shock of such an ejection, indirectly observable already in the Carrington event via the sudden commencement of its geomagnetic storm (**Figure 3**), definitely accelerates SEPs via mechanisms independent of the flare processes themselves. Indeed, acceleration of MeV particles may absorb a substantial fraction of the total event energy (Mewaldt et al. 2005).

Terrestrial (and lunar) material (trees, rocks, etc.) contains embedded radioisotope signatures, notably for our purposes ^{14}C and ^{10}Be, created as secondary emissions from nuclear interactions of solar particles with ambient material (e.g., Usoskin 2017). In particular, ^{14}C allows the dating of such an event via its take-up in trees through dendrochronology, taking advantage of the half-life of $(5.37 \pm 0.04) \times 10^3$ years. Two recently discovered ^{14}C events (Miyake et al. 2012, 2013; ca. 774 and 994 AD) seem likely to have come from SEPs, in which case the remarkable particle fluences they record would suggest a solar event definitely greater in magnitude than the Carrington event. **Figure 11** shows the first of these two events, based on 1-year samples; on this timescale one can see a sudden increase, followed by a long decay consistent with our knowledge of the terrestrial carbon cycle (Usoskin et al. 2013, in a paper subtitled "The Sun Is to Blame"). From this, one can get a feeling about the uncertainty of the conclusion about the origin of this event, but one can also see that a few events in the same year might have conspired to appear together (Section 5.4) as one at the limited time resolution of the sampling and with the blurring effect of the atmospheric circulation of the radioactivity, which begins in the upper atmosphere via an (n,p) reaction on ^{14}N.

The 774 AD tree-ring event, assuming it originated in a single extreme flare and/or CME event, clearly would stand out by comparison with modern data, especially in view of the discovery of ^{10}Be signatures in both (Mekhaldi et al. 2015). They, as well as the Carrington event, whet our appetite for any knowledge of solar extreme events. This implies a harder spectrum than that of modern-era SPE. Usoskin et al. (2020) have reexamined the data for SOL1956-02-23, which was the most powerful modern event (Meyer et al. 1956) and one involved with the remarkable history of the neutron monitor (Simpson 2000). In this context, it is worth noting that the Carrington event did not reveal itself in the radioisotope record, although an early report caused some excitement

regarding the related signature of nitrates in ice cores. With this disappointment, we have no clear way to link recent events with the radioisotope detections; according to a recent analysis (E. Cliver, personal communication), the energy of the 774 AD event was within the same order of magnitude as that of the Carrington event.

Recently O'Hare et al. (2019) have reported a third prehistoric event (~660 BC), this one with signatures in ^{36}Cl as well as ^{10}Be and ^{14}C. Again, this event appeared to have a harder SPE spectrum than any modern event, except perhaps SOL1956-02-23, but one comparable with the other radioisotope events.

5. SOLAR AND/OR STELLAR FLARES AND CORONAL MASS EJECTIONS

5.1. Sunspots and Star Spots

The photometric time series in **Figures 9** and **10** make it clear that sunspots and star spots have some relationship with stellar magnetic activity. Physically one would not expect a direct correlation between spottedness and flare occurrence. Although both depend upon the magnetic field, they depend upon different properties—on the Sun, a sunspot umbra forms at a well-defined magnetic intensity, about 1,867 G (Jurčák 2011). However, a flare strongly favors a location determined by the gradients of the field (e.g., Schrijver 2016). Despite this important qualitative distinction, and the very different physics of the photosphere and corona, the spot group area and flare magnitude both scale with magnetic flux. A gross correlation between spot area and flare magnitude does exist (**Figure 12**), but at any given group area, the whole power law (Section 5.3) of flare magnitudes occurs.

This correlation underpins the modeling of the *Kepler* superflares (Aulanier et al. 2013, Shibata et al. 2013), in which the authors attempt to establish upper limits on the energy of solar flares.
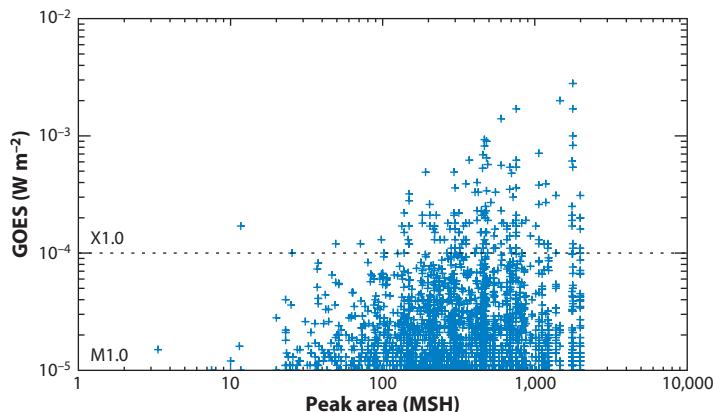
Figure 12

The correlation between the peak GOES fluxes for M- and X-class flares with the areas of their sunspot groups, as estimated from the NOAA listings as accessed through SolarSoft (Freeland & Handy 1998) and covering the time range from August 25, 1991, to October 20, 2017. Note that this restriction to M- and X-class flares represents the nature correlation more correctly than the usual representation (for example, Shibata et al. 2013, their figure 2), which includes weaker C-class events and thus has a selection bias (Wheatland 2001). Abbreviations: GOES, *Geostationary Orbiting Environmental Satellite*; MSH, millionths of solar hemisphere; NOAA, National Oceanic and Atmospheric Administration.

Unfortunately, the frequently quoted correlation (Sammis et al. 2000) has a strong selection bias, resulting from the underreporting of weaker GOES events owing to higher background levels during active times (Wheatland 2010). The less-biased correlation shown in **Figure 12**, for M- and X-class flares only, shows a different pattern. For any given spot area, we get the same power-law distribution of flare magnitudes (Section 5.3). In a well-documented case, for example, Hudson et al. (1992) reported an impulsive X-class white-light flare, SOL1991-12-03, from an active region with negligible spot area. Note also that Dodson & Hedeman (1970) described a list of well-observed major Hα flares in regions with small (or no) spots. These spotless events mainly consist of filament-eruption (**Figure 6**) events in the quiet Sun (Olivieri 1948, Harvey et al. 1986) and/or stealth CMEs (Robbrecht et al. 2009) rather than Carrington events.

5.2. Stellar Coronal Mass Ejections and Solar Energetic Particles?

A major solar event typically consists of a flare, a CME, and the acceleration of SEPs ranging up to relativistic particle energies. Huge geomagnetic effects may ensue, as noted in the context of the Carrington event, resulting from Earth currents induced by ionospheric current systems enhanced by flare effects. Since Carrington's day, we find ourselves with vital infrastructure (and human travel) in space, where the SEPs may cause yet other problems. How analogous stellar CMEs and SEPs might affect the habitability of exoplanets, via whatever mechanisms, therefore motivates us to explore how these phenomena may scale between the solar and stellar cases. The most powerful CMEs tend to have the highest speeds (Stewart et al. 1974a,b; Kahler 1992). For reference, the 17-h travel time (as opposed to days) for the Carrington event corresponds to a bulk velocity of 2.4×10^3 km s^{-1}, corresponding already to a proton energy of some 40 keV even without considering particle acceleration explicitly; as noted above, the particles themselves may absorb a major fraction of the total event energy (e.g., Mewaldt et al. 2005, Chollet et al. 2010). The fraction ranges up to 10% for particle energies above 1 MeV, but the estimations are difficult and model-dependent. For reference, a 1-MeV proton is many decades above the Rosseland–Pannekoek potential or the ambient coronal value of kT. In this respect, ICMEs and SEPs may have a close connection, as expected in view of particle acceleration in the global shock waves driven by the CMEs (e.g., Reames 1999).

We note that the flare–CME relationship has had controversial aspects even in the solar case. For more powerful events, the probability of association tends toward one-to-one (e.g., Yashiro et al. 2005). Indeed, Meng et al. (2019) give some basic statistics for flare and/or CME associations for the superstorm geomagnetic perturbations over the modern era, 1958–2018: no events associated with stealth CMEs, 5% C-class flares, 35% M-class, and 54% X-class, using the ABCMX scale defined previously. Accordingly, we can rely upon flare occurrence as a proxy for CME occurrence—and their stellar weather implications for life—for truly solar-type stars at least.

Unfortunately, stellar CMEs have few unambiguous observables, because by definition we must look to the coronagraph to define CME occurrence, and comparable stellar observations do not exist. Of course, the Sun offers us several proxies (e.g., Hudson & Cliver 2001) closely related to the definitive coronagraph observation of a CME, but almost all are difficult or impossible in the stellar case. The easiest-to-access stellar proxy information comes from the Hα line profile, which (via solar imaging spectroscopy) can nicely show a prominence eruption, surge, or spray; however, these have a complex relationship with one another and with actual CMEs. Leitzinger et al. (2020) have asked the basic question, Can a flare be detected in Sun-as-a-star Hα observations? The

answer is not easily; for the extremely powerful solar flare SOL2003-11-04, the Hα brightness increase was only about 0.2%.

Doppler signatures might also reveal a stellar CME via Hα spectroscopy. Solar CMEs often entrain the material of a prominence, and this cold material can attain high radial velocities (e.g., Gopalswamy 2015). But could one detect a solar CME in Sun-as-a-star spectroscopy in this manner? Apparently not; Vida et al. (2019) have done a large survey for line asymmetries in Hα and other lines for many late-type stars, but they do not describe this kind of phenomenon. Moschou et al. (2019) also describe a wide variety of stellar ejecta but typically not from solar-type stars. Thus, in the stellar literature, one sometimes finds the term CME used to refer to Doppler-shifted Hα line profiles. This is misleading, because a CME is a solar phenomenon observed coronagraphically; even in the solar case, the proxy attributions can cause confusion (e.g., Hudson & Cliver 2001). A CME of course leads to interplanetary signatures (the ICME defined above), but there remains some uncertainty about relating the coronagraphic and direct imaging domains. The solar corona does not emit much Hα radiation, and there appears to be no literature describing Sun-as-a-star detection of the counterparts of actual solar CMEs in Hα.

The EUV dimming signature probably tops the list of likely proxy methods for CME detection on remote stars (e.g., Harra et al. 2016). This became apparent in the EUV Variability Experiment (EVE) Sun-as-a-star EUV observations (Woods et al. 2012). In this signature, the mass removed from the corona by the CME can deplete the solar corona by as much as 10% as observed coronagraphically (see the example shown in **Figure 5**). The dimming signature also prominently appears in soft X-ray images (e.g., Hudson & Webb 1997), but its detection requires imaging; the soft X-ray emission of the flare obliterates the dimming in Sun-as-a-star mode. In the EUV, after the flare emissions in high-temperature lines, such as those of Fexx–xxiv, a distinct dimming signature appears in the lower ionization states, such as Feviii–xiii (Hock et al. 2012, Harra et al. 2016, Mason et al. 2016). **Figure 13** illustrates this and some other attributes of the EUV flare spectrum that might be carried over into the stellar domain, given good enough observational material.

Strikingly, this figure shows large depressions in the lines of low-excitation ions. This is readily identifiable as the coronal X-ray dimming associated with a CME (see the sidebar titled Detectability of Stellar Coronal Mass Ejections via Dimming). In this case the total volumetric emission measure decreased by about 10%, and the Sun provided enough signal for easy detection in a single 10-s snapshot spectrum. Other flare attributes here include the signature of the hot flare loops (e.g., Fexix–xxiv), the "EVE late phase" (Woods et al. 2011) becoming dominant at Fexv, and the dimming at Fexii and below. Note also the impulsive phase, visible across a wide range of excitation states and clearly distinguishable just before the GOES peak time, for example, in the Fexii trace. This represents the thick-target footpoint excitation (e.g., Neupert 1989) also extending to the soft X-ray range (McTiernan et al. 1993, Hudson et al. 1994).

5.3. The Power Law

Solar flares follow a clearly defined power-law distribution in magnitude, as noted early by Akabane (1956) via microwave burst data. Many other observables follow approximately the same power law, notably soft (Drake 1971) and hard (Crosby et al. 1993) X-ray bursts. **Figure 14** shows an exceptionally clean example of one set of observations from Crosby et al. (1993). This power law extends over three decades in flare peak flux, but crucially the distribution suggests a rollover at the high end, with possible physical implications as discussed below. The rollover at the low end reflects selection bias and, thus, has no particular significance (see Kashyap et al. 2002 for a discussion of relevance to coronal heating). Many other phenomena across nature
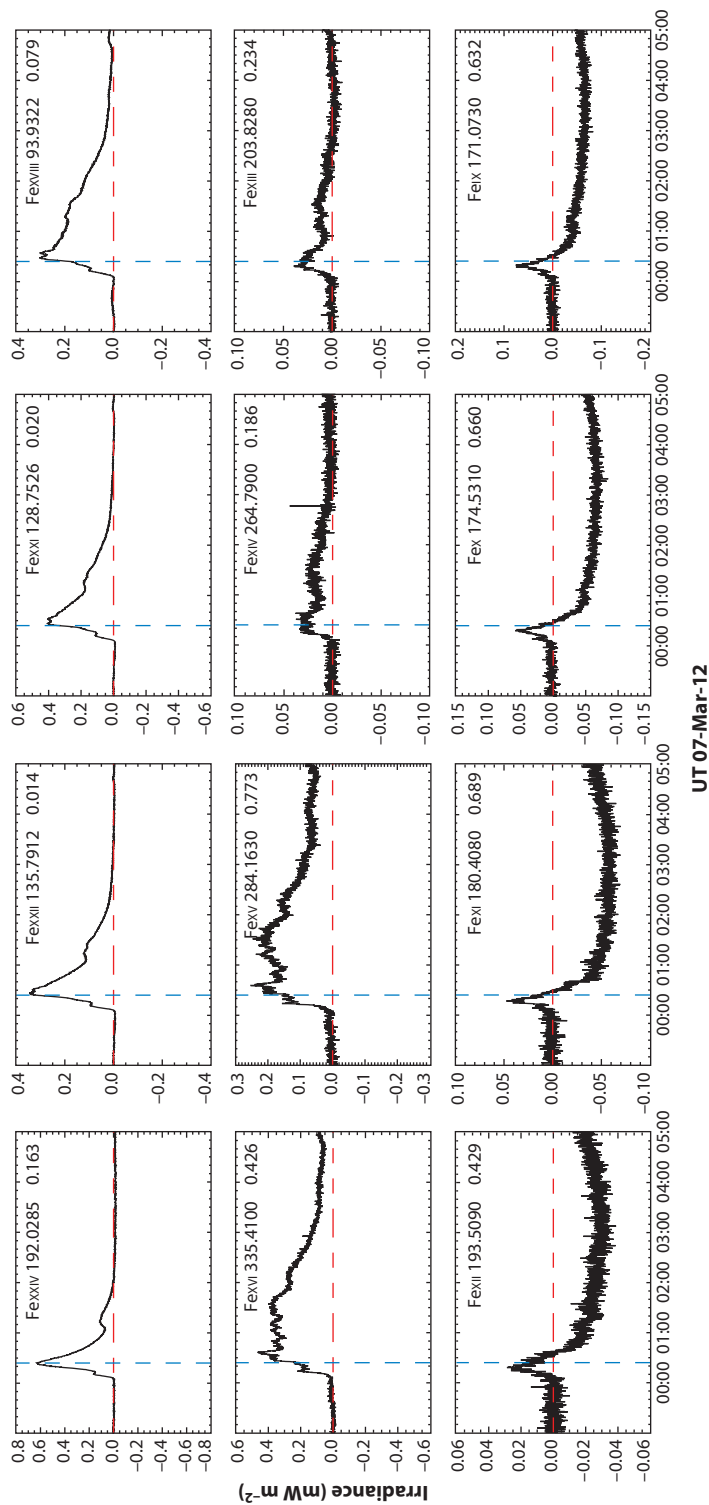
Figure 13

A major solar flare observed in many Fe emission lines in the EUV by the EVE instrument on SDO. Each panel is a six-hour time series, with the lines arranged by temperature of formation from upper left (flare temperatures) to lower right (quiet-Sun temperatures). The time series have preflare fluxes subtracted and show just the flare excess, with normalization value shown on the titles. Sample interval 10 s; the vertical dashed line shows the GOES 1–8-Å peak time (cf. Harra et al. 2016). Abbreviations: EUV, extreme ultraviolet; EVE, EUV Variability Experiment; GOES, Geostationary Orbiting Environmental Satellite; SDO, *Solar Dynamics Observatory*.

DETECTABILITY OF STELLAR CORONAL MASS EJECTIONS VIA DIMMING

Dimming

A stellar CME can show up as a brightness deficit in a well-detected coronal wavelength, but this is unambiguous if that wavelength does not have strong competition from flare emission. This simple signature does not have the diagnostic strength of line profile observations, but in some spectral bands it may have a high signal-to-noise ratio.

The Extreme Ultraviolet

In the EUV spectral band of 50–300 Å, one has a library of Fe emission lines that show the solar corona in quiescent and disturbed conditions, and with the well-defined dimming signature betraying CME occurrences.

Limitations

A solar dimming may reduce the coronal signal by as much as 10% and persist for several hours. Successful stellar observations would therefore need a signal-to-noise ratio of roughly 100 in about one hour's integration for a good 10σ detection. Interstellar extinction strongly limits the volume of space accessible to this technique.

(famously, earthquakes) show similar power-law occurrence distributions behavior (e.g., McAteer et al. 2016). The link to $1/f$ noise in this behavior led to models of self-organized criticality (Bak et al. 1987, Aschwanden 2019), as introduced to flare physics by Lu & Hamilton (1991).

The power-law occurrence pattern appears in various observables, but from a theoretical point of view one might wish to interpret these as proxies for the total energy of an event. Unfortunately, the observables each sample some part of the process in a complicated model-dependent manner; the structure that flares typically involves orders-of-magnitude inhomogeneities that defy any
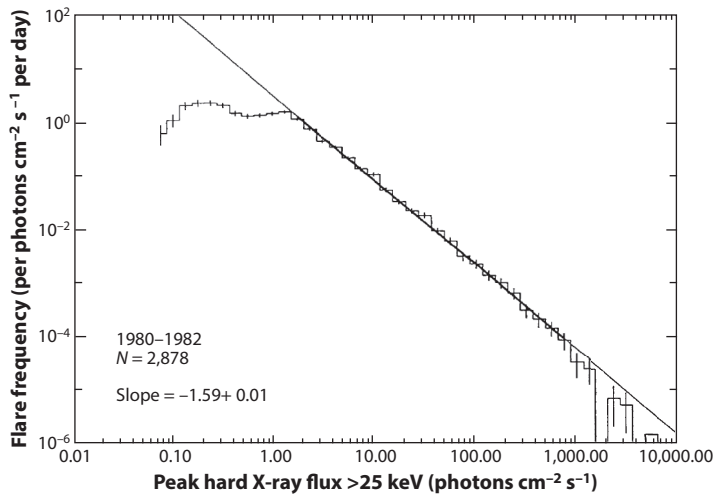
Figure 14

Peak fluxes of solar hard X-ray flares at energies above 25 keV. During this observing interval (1980–1982) about 107 GOES X-class flares occurred. The power-law fit refers to the higher-energy events, and the discrepancy below the extrapolation to lower energies reveals the detection limit. Figure adapted with permission from Crosby et al. (1993); copyright 1993 Springer Nature B.V. Abbreviation: GOES, *Geostatic Orbiting Environmental Satellite*.
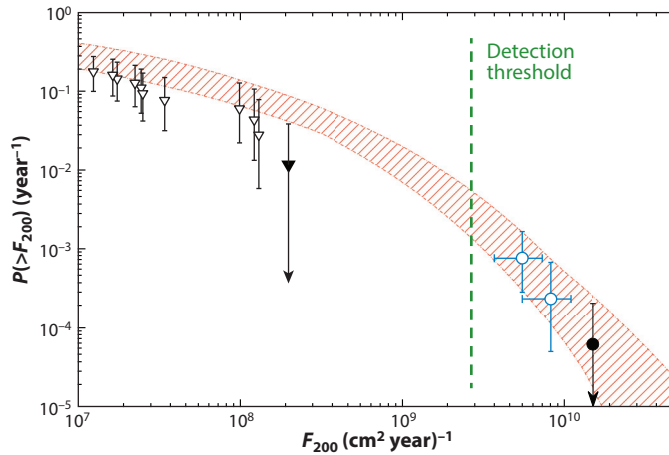
Figure 15

Integral distribution function of yearly fluences of solar protons (i.e., SEPs) above 200 MeV, with triangles showing the space-era data and circles the radioisotope results; filled symbols are upper limits, and the hatched band shows a fitted Weibull distribution with 68% uncertainties (cf. Miyake et al. 2019, their figure 6.15). Figure provided by I. Usoskin. Abbreviation: SEPs, solar energetic particles.

description in terms of typical or average values of physical parameters. The inference of total event energy from any one of these observables thus has ill-defined uncertainties. The soft X-ray emission (GOES photometry), for example, carries only a small fraction of the total energy (e.g., Shimizu 1995). White-light emission from a solar or stellar flare (e.g., for the Carrington flare) as described in Section 2 can contain a much larger energy fraction but, again, in a model-sensitive manner. In the solar case, we cannot detect any optical continuum from the photosphere or chromosphere for individual weak white-light flare events even in the best imaging observations because of natural photospheric fluctuations caused by convection and oscillations (Hudson 1988); see Section 5.4 for a quantitative view of this kind of limitation in the stellar or Sun-as-a-star case.

In accepting the power-law scaling of some proxy variable to describe the total event energy distribution, a further problem arises. For a distribution in total energy $dN/dW \propto W^{-\gamma}$, many studies have found $\gamma < 2$; for example, Crosby et al. (1993) reported a quite precise value of 1.59 ± 0.01 over some three decades of peak hard X-ray fluxes (**Figure 14**). If such a flat power law truly describes the energy release, then the biggest events dominate the total energy—the integral over the distribution does not converge (Collura et al. 1988, Hudson 1991). We would thus require a rollover at some finite flare energy, as yet not identified robustly in a global sense (cf. Kucera et al. 1997).

Figure 15 shows the distribution of SEPs fluences, integrating modern space-based direct observations with the fossil record. Cosmogenic radioisotope evidence can be gleaned from lunar rocks as well as terrestrial sources such as tree rings. Depending upon the half-life of the isotope, one can even look through the ages in a search for major SEPs fluences (Reedy & Arnold 1972). The striking result of a high-end rollover in the SEPs fluences inferred in this way, originally by Lingenfelter & Hudson (1980) from ^{14}C records, calls to mind the idea of a rollover in the distribution of solar flare magnitudes.

5.4. A Latter-Day Solar Carrington Event?

The patterns of solar activity have strong correlations in both space and time, such as the butterfly diagram (Maunder 1904). On shorter timescales, the statistical pattern described as "nests
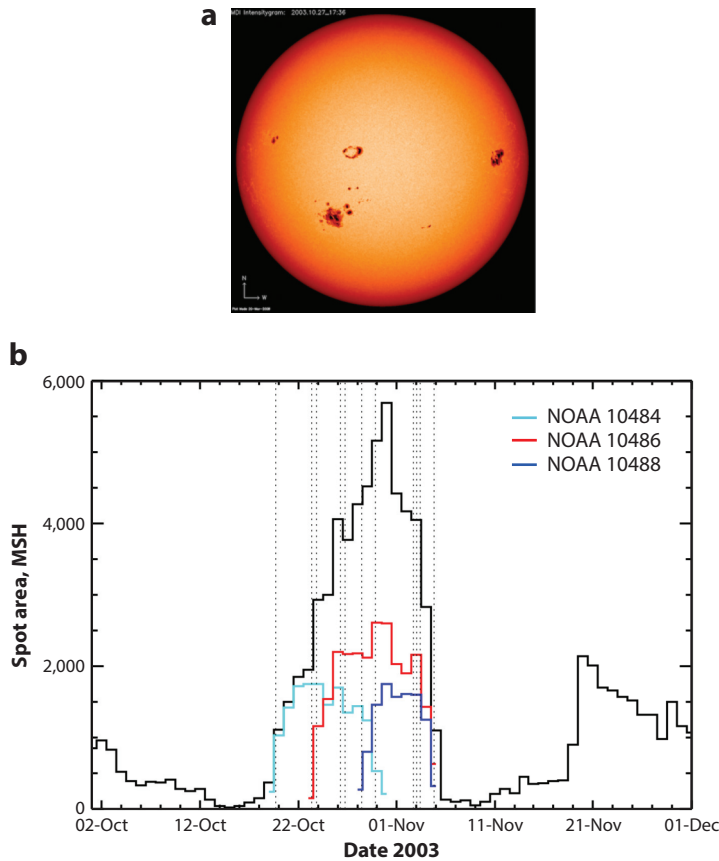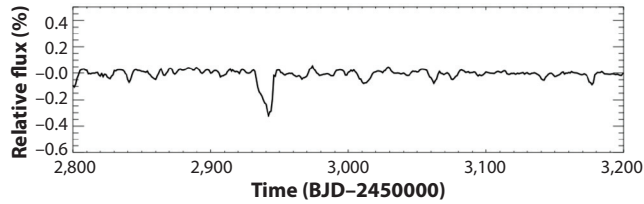
Figure 16

(*a*) The sunspots of October 28, 2003. (*b*) Sunspot group areas for three solar rotations around this time, with vertical dotted lines at times of major (GOES X-class) flares. Abbreviations: GOES, *Geostationary Orbiting Environmental Satellite*; MSH, millionths of solar hemisphere; NOAA, National Oceanic and Atmospheric Administration.

of activity" appears (Zwaan 1987). This matches the dictum that magnetic flux tends to emerge where other flux has already emerged, and suggests a window on the coherent subphotospheric organization of the interior dynamo field.

This organization may extend to spatial scales larger than the network scale and even perhaps crossing the equator. **Figure 16** shows the Halloween flare epoch of October–November 2003, and specifically the flare SOL2003-10-28 detected bolometrically via the TSI measurements (Kopp et al. 2005). During the time covered (about three rotations), three large sunspot groups emerged within about one week, two in the northern hemisphere and one in the southern, each producing major flares.

Setting aside the weakness of the SEPs and/or flare scaling, the two tree-ring ^{14}C events discovered by Miyake et al. thus have another basic problem as we try to infer their significance in solar event history: the long circulation time of carbon in the terrestrial environment. This means that events occurring closely in time, where closely means within months of one another, can

Figure 17

Solar bolometric total solar irradiance variations during the Halloween flare epoch (**Figure 16**). Note the absence of any hint of periodicity, plus the lack of rotational recurrence of the major dip associated with the three large sunspot groups. This dip lacks symmetry because of their simultaneous presence; for an isolated sunspot, the dip has a duration of about one week. Figure adapted from Işık et al. (2020); copyright 2020 Oxford University Press.

produce a composite event that could mimic a single superflare occurrence. Radioisotope proxies do not have the time resolution to distinguish multiple events; for ^{14}C, the Halloween events would merge together and appear as a single episode. Here, the net sunspot area at maximum approached 6,000 MSH, an area greatly exceeding that of the Carrington region, and the flares of that week, added together, reached a GOES classification of order X100, which is significantly greater than estimates for the Carrington flare. The solar particle event ranked fourth in magnitude among SPEs since 1976, and the geomagnetic storm ranked sixth since 1932 (Balch et al. 2004); see Cliver & Svalgaard (2004) for further comparisons.

How would this Carrington-class composite of activity appear to a stellar astronomer? **Figure 17** shows a time series of TSI converted into photometric units; the time series shows one major dip, which does not recur despite an apparent conflict with the Gnevyshev–Waldmeier relation for sunspot groups: $A = (13.0 \pm 1.1) \times T$, with A being the maximum area of a spot group in MSH and T its total observable lifetime in days (Nagovitsyn et al. 2019). This predicts a lifetime of many months for a spot group with the inferred area of the Carrington group, but it refers to its likely visibility in high-resolution images rather than in the TSI measurement as limited by the broad-band noise visible in **Figure 17**. There is no hint in the solar photometry of the near-sinusoidal variation shown by more rapidly rotating *Kepler* solar-type stars (**Figure 9**).

6. IMPLICATIONS

6.1. Stellar

Thanks especially to the *Kepler* observatory, we now have excellent time-series photometry from space for a large number of stars, including many across the spectrum that show flaring. As introduced above, these stellar events include superflares on apparently solar-type objects based on mass, effective temperature, rotation period, and other physical properties. Do events of the Carrington flare's magnitude occur on these stars, and can we use their occurrence statistics to help assess the risk of future solar extreme events? The most recent discussion of these questions (Notsu et al. 2019) is illustrated in **Figure 18**, the occurrence of flares at estimated energies above 5×10^{34} erg (crudely, 100× the energy of the Carrington event) as a function of rotation period. In spite of the excellent data, **Figure 18** shows that we remain at the mercy of weak statistics in the face of strong dependences upon surface temperature and rotation period. At this flare energy, in fact, there were no events at all for rotation periods longer than about 15 days; the authors nevertheless state that such events occur approximately once every 2,000–3,000 years. This
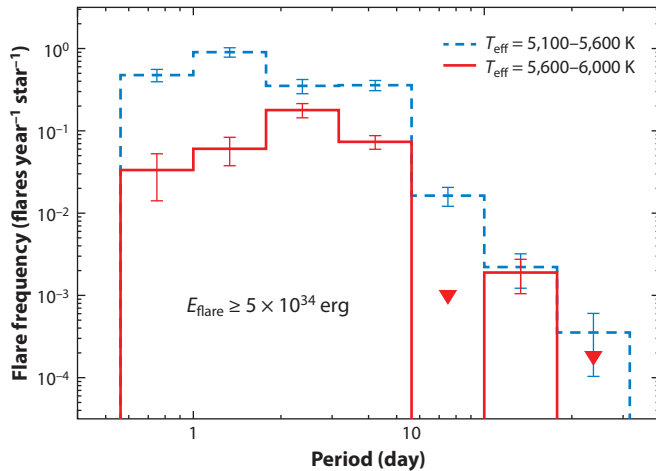
Figure 18

The occurrence rates for stellar superflares with $\sqrt{N}$ uncertainties, for solar-type stars. Note the decrease of superflare occurrence with increasing rotation period, and absence of superflares at the solar rotation period of about 25 days and for the solar surface temperature sample (*red*). Figure adapted with permission from Notsu et al. (2019); copyright 2019 Springer Nature B.V.

situation may change; Tu et al. (2020) comment that TESS data also are insufficient at present, at solar rotation periods, but we can certainly hope for more complete statistics in the future.

The inference of a solar superflare likelihood, as described above, could still be consistent with the new data if the solar occurrence power law extends to this level. This may not happen; as described in Section 5.3, it seems likely that the power law steepens just about at the presently observable range, and the SEPs radioisotope record backs this up given the (strong) further assumption that SEPs and flare energy scale together for events of these magnitudes (cf. Aarnio et al. 2014). A pessimist could also note, as described in Section 5.4, that the Miyake events (assumed to be solar) do not require an explanation in terms of single isolated extreme flare and/or CMEs. By contrast, exact characterization of the total energy of a solar flare remains quite uncertain, and the stellar data have severe limitations on top of that, and so it may well turn out eventually that the *Kepler* superflare data do connect with the solar observations. This reasonable possibility remains speculative at present.

The simple power-law dependence, if extrapolated, allows for a straightforward estimation of solar superflare occurrence (e.g., Love 2012). But we have noted the likelihood that a rollover occurs, and if so this extrapolation has no firm basis. This does not mean that we can dismiss superflare occurrence entirely. Independent of the observed flare statistics, dominated by the power law, a different physical basis for extreme events might well exist. This is the Dragon-King possibility (Sornette & Ouillon 2012), and the most extreme events may help guide us to hints about this uncommon physics. The exceptionally hard SEP spectrum of SOL1956-02-23, comparable with the spectra inferred from the radioisotope detections, hints that these events might belong to such a class.

6.2. Space Weather

Two of the three main paths for solar-terrestrial geoeffectiveness (SEPs in near-Earth space, and Earth currents driven by magnetic storms) have complicated relationships with the solar

THREE PATHS OF GEOEFFECTIVENESS

■ Electromagnetic (the flare via X-rays and γ-rays)
■ The SEPs, including prompt relativistic particles
■ The magnetized plasma cloud of the ICME.

In the solar case, these have only weak scaling relationships, and extrapolation to any stellar environment has uncertainty

sources, because they depend upon heliospheric and terrestrial conditions as well as the initial impetus (see the sidebar titled Three Paths of Geoeffectiveness).[7] Our new-found insights from radioisotopes and stellar flares do not add to our understanding of how these relationships might work in more extreme events, because we naturally have no information about SEPs or CMEs for these events. At the Carrington level, comparable events have occurred (e.g., Hayakawa et al. 2017, Hapgood 2019, Love et al. 2019). The recent solar backside event SOL2012-07-23 had an ICME transit time of only 19 hours, which is not so different from that of the Carrington event, and Baker et al. (2013) argue that the heliospheric environment at that time could have produced an even greater geomagnetic storm were it to have occurred on the visible hemisphere of the Sun.

7. CONCLUSIONS

The Carrington event ignited our interest in understanding solar extreme events for space weather, as summarized via the three main channels of hazard: the flare radiation directly, the geomagnetic consequences, and the associated SEPs.

Two of the Halloween solar flares of October–November 2003 each had total radiated energies comparable with that of the Carrington flare: SOL2003-11-28 and SOL2003-11-04 via direct bolometric detection (Emslie et al. 2012), and SOL2004-11-04 also via its geomagnetic crochet signature (Curto et al. 2016). Thus, from the solar point of view, the Carrington event only marginally deserved the term superflare, possibly achieving our criterion of 10^{33} erg within the range of uncertainty. From the geomagnetic point of view of geoeffectiveness, from which we have only sketchy ideas of how to relate this to the radiated energy of the flare, the Carrington magnetic storm may also not have been particularly exceptional.

A new Carrington event therefore does not suggest an energy scale that would pose a major threat to humankind, for example, although another similar event could surprise us; Baker et al. (2013) pointed out that a huge solar event in July 2012 occurred on the solar hemisphere facing away from Earth, and it could have had a serious impact on Earth but for that fact. In terms of nineteenth-century natural disasters, the Mount Tambora volcanic eruption of 1815 had far more important consequences than the Carrington event. This eruption ejected an estimated 1.4×10^{17} g of material into Earth's atmosphere (Oppenheimer 2003) and thus created "the year without a summer," easily outdoing the Carrington event in terms of geoeffectiveness—for roughly the same ejected mass—that is, volcanic ash, not high-temperature ionized plasma.

---

[7]The Carrington event certainly planted the seed for the ultimate development of our understanding of space weather. Shea & Smart (2006) provide an interesting discussion of how the contemporaneous astronomer E. Loomis had explored the remarkable terrestrial effects of this flare.

SUMMARY POINTS

1. The Carrington event of 1859 led to many developments in astrophysics, and specifically to what we now call multimessenger astronomy, time-domain astronomy, and even high-energy astrophysics.

2. The flare itself, though powerful, did not significantly exceed the magnitudes of the greatest events observed in the modern era.

3. Stellar superflare events on solar-type stars may share common paradigms with solar flares, suggesting the possibility of more extreme solar events in the future.

DISCLOSURE STATEMENT

The author is not aware of any affiliations, memberships, funding, or financial holdings that might be perceived as affecting the objectivity of this review.

ACKNOWLEDGMENTS

LITERATURE CITED

Aarnio AN, Stassun KG, Matt SP. 2014. In *Nature of Prominences and Their Role in Space Weather, Proc. IAU Symp. 300*, Vol. 8, ed. B Schmieder, JM Malherbe, ST Wu, pp. 318–21. Cambridge, UK: Cambridge Univ. Press

Akabane K. 1956. *Publ. Astron. Soc. Jpn.* 8:173

Aly JJ. 1991. *Ap. J. Lett.* 375:L61–64

Anderson KA, Winckler JR. 1962. *J. Geophys. Res.* 67:4103–17

Aschwanden MJ. 2019. *Ap. J.* 880:105

Aschwanden MJ, Caspi A, Cohen CMS, et al. 2017. *Ap. J.* 836:17

Aulanier G, Démoulin P, Schrijver CJ, et al. 2013. *Astron. Astrophys.* 549:A66

Bak P, Tang C, Wiesenfeld K. 1987. *Phys. Rev. Lett.* 59:381–84

Baker DN, Li X, Pulkkinen A, et al. 2013. *Space Weather* 11:585–91

Balch CC, Crown MD, Viereck R. 2004. In *American Astronomical Society Meeting 204*, id.02.19 (Abstr.)

Bartels J. 1937. *Terr. Magn. Atmos. Electr. (J. Geophys. Res.)* 42:235–39

Bastien FA, Stassun KG, Basri G, Pepper J. 2013. *Nature* 500:427–30

Boteler DH. 2006. *Adv. Space Res.* 38:159–72

Bradshaw SJ, Mason HE. 2003. *Astron. Astrophys.* 407:1127–38

Bratenahl A, Baum PJ. 1976. *Solar Phys.* 47:345–60

Brown JC. 1971. *Solar Phys.* 18:489–502

Bruzek A. 1964. *Ap. J.* 140:746–59

Burlaga LF, Klein L, Sheeley NRJ, et al. 1982. *Geophys. Res. Lett.* 9:1317–20

Cargill PJ, Mariska JT, Antiochos SK. 1995. *Ap. J.* 439:1034–43

Carlsson M, Stein RF. 1997. *Ap. J.* 481:500–14

Carmichael H. 1964. *NASA Spec. Publ.* 50:451–56

Carrington RC. 1859. *MNRAS* 20:13–16

Chen PF. 2011. *Living Rev. Solar Phys.* 8:1

Chollet EE, Giacalone J, Mewaldt RA. 2010. *J. Geophys. Res. (Space Phys.)* 115:A06101

Clark S. 2007. *The Sun Kings: The Unexpected Tragedy of Richard Carrington and the Tale of How Modern Astronomy Began.* Princeton, NJ: Princeton Univ. Press

Cliver EW, Dietrich WF. 2013. *J. Space Weather Space Clim.* 3:A260000

Cliver EW, Kahler SW, Kazachenko M, Shimojo M. 2019. *Ap. J.* 877:11

Cliver EW, Keer NC. 2012. *Solar Phys.* 280:1–31

Cliver EW, Svalgaard L. 2004. *Solar Phys.* 224:407–22

Collura A, Pasquini L, Schmitt JHMM. 1988. *Astron. Astrophys.* 205:197–206

Cranmer SR. 2017. *Ap. J.* 840:114

Crosby NB, Aschwanden MJ, Dennis BR. 1993. *Solar Phys.* 143:275–99

Curto JJ. 2020. *J. Space Weather Space Clim.* 10:27

Curto JJ, Castell J, Del Moral F. 2016. *J. Space Weather Space Clim.* 6:A23

Davis R Jr. 1993. In *Frontiers of Neutrino Astrophysics*, ed. Y Suzuki, K Nakamura, pp. 47–60. Tokyo: Univ. Acad.

Dellinger JH. 1936. *Phys. Rev.* 50:1189

Desai M, Giacalone J. 2016. *Living Rev. Solar Phys.* 13:3

Dodson HW. 1961. *PNAS* 47:901–5

Dodson HW, Hedeman ER. 1970. *Solar Phys.* 13:401–19

Drake JF. 1971. *Solar Phys.* 16:152–85

Dungey JW. 1994. *J. Geophys. Res.* 99:19189

Emslie AG, Dennis BR, Shih AY, et al. 2012. *Ap. J.* 759:71

Field GB. 1965. *Ap. J.* 142:531–67

Fletcher L, Dennis BR, Hudson HS, et al. 2011. *Space Sci. Rev.* 159:19–106

Fletcher L, Hudson HS. 2008. *Ap. J.* 675:1645–55

Freeland SL, Handy BN. 1998. *Solar Phys.* 182:497–500

Gaizauskas V, Švestka Z. 1987. *Solar Phys.* 114:389–98

Georgoulis MK, Titov VS, Mikić Z. 2012. *Ap. J.* 761:61

Giovanelli RG. 1946. *Nature* 158:81–82

Gopalswamy N. 2015. In *Astrophysics and Space Science Library*, Vol. 415: *Solar Prominences*, ed. JC Vial, O Engvold, pp. 381–410. Cham, Switz.: Springer Int.

Graham G. 1724. *Philos. Trans. R. Soc. Lond. Ser. I* 33:96–107

Hapgood M. 2019. *Space Weather* 17:950–75

Harra LK, Schrijver CJ, Janvier M, et al. 2016. *Solar Phys.* 291:1761–82

Harvey KL, Sheeley NR Jr., Harvey JW. 1986. In *Solar-Terrestrial Predictions: Proceedings of a Workshop at Meudon, France, June 18–22, 1984*, ed. PA Simon, G Heckman, MA Shea, p. 198. Washington, DC: Natl. Ocean. Atmos. Admin.

Hayakawa H, Ebihara Y, Willis DM, et al. 2019. *Space Weather* 17:1553–69

Hayakawa H, Iwahashi K, Ebihara Y, et al. 2017. *Ap. J. Lett.* 850:L31

Heyvaerts J, Priest ER, Rust DM. 1977. *Ap. J.* 216:123–37

Hirayama T. 1974. *Solar Phys.* 34:323–38

Hock RA, Chamberlin PC, Woods TN, et al. 2012. *Solar Phys.* 275:145–78

Hodgson R. 1859. *MNRAS* 20:15–16

Hudson H, Ryan J. 1995. *Annu. Rev. Astron. Astrophys.* 33:239–82

Hudson HS. 1972. *Solar Phys.* 24:414–28

Hudson HS. 1988. *Annu. Rev. Astron. Astrophys.* 26:473–507

Hudson HS. 1991. *Solar Phys.* 133:357–69

Hudson HS. 2000. *Ap. J. Lett.* 531:L75–77

Hudson HS. 2011. *Space Sci. Rev.* 158:5–41

Hudson HS. 2016. *Solar Phys.* 291:1273–322

Hudson HS, Acton LW, Hirayama T, Uchida Y. 1992. *Publ. Astron. Soc. Jpn.* 44:L77–81

Hudson HS, Cliver EW. 2001. *J. Geophys. Res.* 106:25199–214

Hudson HS, Strong KT, Dennis BR, et al. 1994. *Ap. J. Lett.* 422:L25–27

Hudson HS, Svalgaard L. 2019. *Phys. Today* 72:10–12

Hudson HS, Webb DF. 1997. *Washington DC Am. Geophys. Union Geophys. Monogr. Ser.* 99:27–38

Hudson HS, Woodard MF. 1983. *Bul. Am. Astron. Soc.* 15:715

Işık E, Shapiro AI, Solanki SK, Krivova NA. 2020. *Ap. J. Lett.* 901:L12

Janvier M, Aulanier G, Pariat E, Démoulin P. 2013. *Astron. Astrophys.* 555:A77

Jefferies JT, Orrall FQ. 1961. *Ap. J.* 133:963–68

Jejčič S, Kleint L, Heinzel P. 2018. *Ap. J.* 867:134

Jurčák J. 2011. *Astron. Astrophys.* 531:A118

Kahler SW. 1992. *Annu. Rev. Astron. Astrophys.* 30:113–41

Kahler SW, Hudson HS. 2001. *J. Geophys. Res.* 106:29239–48

Kane SR, Donnelly RF. 1971. *Ap. J.* 164:151–63

Kashyap VL, Drake JJ, Güdel M, Audard M. 2002. *Ap. J.* 580:1118–32

Klimchuk JA, Patsourakos S, Cargill PJ. 2008. *Ap. J.* 682:1351–62

Koch DG, Borucki WJ, Basri G, et al. 2010. *Ap. J. Lett.* 713:L79–86

Kopp G, Lawrence G, Rottman G. 2005. *Solar Phys.* 230:129–39

Kopp G, Lean JL. 2011. *Geophys. Res. Lett.* 380:L01706

Kopp RA, Pneuman GW. 1976. *Solar Phys.* 50:85–98

Kowalski AF, Hawley SL, Carlsson M, et al. 2015. *Solar Phys.* 290:3487–523

Kowalski AF, Hawley SL, Holtzman JA, Wisniewski JP, Hilton EJ. 2010. *Ap. J. Lett.* 714:L98–102

Kucera TA, Dennis BR, Schwartz RA, Shaw D. 1997. *Ap. J.* 475:338–47

Leitzinger M, Odert P, Greimel R, et al. 2020. *MNRAS* 493:4570–89

Lewin WHG, Clark GW, Smith WB. 1967. *Ap. J. Lett.* 150:L153–55

Lingenfelter RE, Hudson HS. 1980. In *The Ancient Sun: Fossil Record in the Earth, Moon and Meteorites, Proceedings of the Conference, Boulder, CO, October 16–19, 1979* (A81-48801 24-91), ed. RO Pepin, JA Eddy, RB Merrill, pp. 69–79. New York and Oxford: Pergamon

Lockwood M. 2013. *Liv. Rev. Solar Phys.* 10:4

Love JJ. 2012. *Geophys. Res. Lett.* 39:10301

Love JJ, Hayakawa H, Cliver EW. 2019. *Space Weather* 17:1281–92

Lu ET, Hamilton RJ. 1991. *Ap. J. Lett.* 380:L89–92

Maehara H, Shibayama T, Notsu S, et al. 2012. *Nature* 485:478–81

Mason JP, Woods TN, Webb DF, et al. 2016. *Ap. J.* 830:20

Maunder EW. 1904. *MNRAS* 64:747–61

McAteer RTJ, Aschwanden MJ, Dimitropoulou M, et al. 2016. *Space Sci. Rev.* 198:217–66

McCracken KG. 1959. *Nuovo Cim.* 13:1081–85

McTiernan JM, Kane SR, Loran JM, et al. 1993. *Ap. J. Lett.* 416:L91–93

Mekhaldi F, Muscheler R, Adolphi F, et al. 2015. *Nat. Commun.* 6:8611

Melrose DB. 1995. *Ap. J.* 451:391–401

Melrose DB. 2017. *J. Geophys. Res. (Space Phys.)* 122:7963–78

Meng X, Tsurutani BT, Mannucci AJ. 2019. *J. Geophys. Res. (Space Phys.)* 124:3926–48

Mewaldt RA, Cohen CMS, Mason GM, et al. 2005. In *Solar Wind 11/SOHO 16, Connecting Sun and Heliosphere*, ed. B Fleck, TH Zurbuchen, H Lacoste, pp. 67–70. ESA Spec. Publ. 592. Noordwijk, Neth.: ESA

Meyer P, Parker EN, Simpson JA. 1956. *Phys. Rev.* 104:768–83

Milligan RO, Hudson HS, Chamberlin PC, Hannah IG, Hayes LA. 2020. *Space Weather* 18:e02331

Miyake F, Masuda K, Nakamura T. 2013. *Nat. Commun.* 4:1748

Miyake F, Nagaya K, Masuda K, Nakamura T. 2012. *Nature* 486:240–42

Miyake F, Usoskin I, Poluianov S, eds. 2019. *Extreme Solar Particle Storms: The Hostile Sun*. Bristol, UK: IOP

Moore RL, Sterling AC, Hudson HS, Lemen JR. 2001. *Ap. J.* 552:833–48

Moschou SP, Drake JJ, Cohen O, et al. 2019. *Ap. J.* 877:105

Nagai F. 1980. *Solar Phys.* 68:351–79

Nagovitsyn YA, Ivanov VG, Skorbezh NN. 2019. *Astron. Lett.* 45:396–401

Najita K, Orrall FQ. 1970. *Solar Phys.* 15:176–94

Neidig DF. 1989. *Solar Phys.* 121:261–69

Neupert WM. 1968. *Ap. J. Lett.* 153:L59–64

Neupert WM. 1989. *Ap. J.* 344:504–12

Nevanlinna H. 2006. *Adv. Space Res.* 38:180–87

Newton HW. 1943. *MNRAS* 103:244–57

Newton HW. 1955. *Vistas Astron.* 1:666–74

Notsu Y, Maehara H, Honda S, et al. 2019. *Ap. J.* 876:58

Obayashi T. 1975. *Solar Phys.* 40:217–26

O'Hare P, Mekhaldi F, Adolphi F, et al. 2019. *PNAS* 116:5961–66

Olivieri G. 1948. *L'Astronomie* 62:343

Oppenheimer C. 2003. *Prog. Phys. Geogr.: Earth Environ.* 27:230–59

Parker EN. 1996. *Ap. J.* 471:485–88

Peterson L, Winckler JR. 1958. *Phys. Rev. Lett.* 1:205–6

Prosser S. 2018. *Astron. Geophys.* 59(5):9

Reale F. 2014. *Liv. Rev. Solar Phys.* 11:4

Reames DV. 1999. *Space Sci. Rev.* 90:413–91

Reedy RC, Arnold JR. 1972. *J. Geophys. Res.* 77:537–55

Ricker GR, Winn JN, Vanderspek R, et al. 2015. *J. Astron. Telesc. Instrum. Syst.* 1:014003

Riley P. 2012. *Space Weather* 10:2012

Robbrecht E, Patsourakos S, Vourlidas A. 2009. *Ap. J.* 701:283–91

Rosner R, Tucker WH, Vaiana GS. 1978. *Ap. J.* 220:643–45

Rudaux L. 1892. *L'Astronomie* 11:342–44

Sabine E. 1871. *Philos. Trans. R. Soc. Lond. Ser. I* 161:307–19

Sammis I, Tang F, Zirin H. 2000. *Ap. J.* 540:583–87

Schaefer BE, King JR, Deliyannis CP. 2000. *Ap. J.* 529:1026–30

Schrijver CJ. 2016. *Ap. J.* 820:103

Schrijver CJ, Beer J, Baltensperger U, et al. 2012. *J. Geophys. Res. (Space Phys.)* 117:A08103

Secchi A. 1872. *Compt. Rend. Acad. Sci. Paris* 75:1581

Shea K, Smart H. 2006. *Adv. Space Res.* 38:313–85

Shibata K, Isobe H, Hillier A, et al. 2013. *Publ. Astron. Soc. Jpn.* 65:49

Shibata K, Magara T. 2011. *Living Rev. Solar Phys.* 8:6–99

Shimizu T. 1995. *Publ. Astron. Soc. Jpn.* 47:251–63

Simpson JA. 2000. *Space Sci. Rev.* 93:11–32

Sornette D, Ouillon G. 2012. *Eur. Phys. J. Spec. Top.* 205:1–26

Stewart B. 1860. *Proc. R. Soc. Lond. Ser. I* 11:407–10

Stewart B. 1861. *Philos. Trans. R. Soc. Lond. Ser. I* 151:423–30

Stewart RT, Howard RA, Hansen F, Gergely T, Kundu M. 1974a. *Solar Phys.* 36:219–31

Stewart RT, McCabe MK, Koomen MJ, Hansen RT, Dulk GA. 1974b. *Solar Phys.* 36:203–17

Sturrock PA. 1966. *Nature* 211:695–97

Sturrock PA, ed. 1980. *Solar Flares*. Boulder: Colorado Univ. Press

Sturrock PA. 1991. *Ap. J.* 380:655–59

Sudol JJ, Harvey JW. 2005. *Ap. J.* 635:647–58

Sun X, Hoeksema JT, Liu Y, et al. 2012. *Ap. J.* 748:77

Švestka Z. 1970. *Solar Phys.* 13:471–89

Švestka Z. 1976. *Solar Flares*. Dordrecht, Neth.: Reidel

Syrovatskii SI. 1981. *Annu. Rev. Astron. Astrophys.* 19:163–229

Tarnstrom GL, Zehntner C. 1975. *Nature* 258:693–94

Toriumi S, Wang H. 2019. *Liv. Rev. Solar Phys.* 16:3

Trouvelot EL. 1891. *L'Astronomie* 10:287–89

Tsurutani BT, Gonzalez WD, Lakhina GS, Alex S. 2003. *J. Geophys. Res. (Space Phys.)* 108:1268

Tu ZL, Yang M, Zhang ZJ, Wang FY. 2020. *Ap. J.* 890:46

Usoskin IG. 2017. *Liv. Rev. Solar Phys.* 14:3

Usoskin IG, Koldobskiy SA, Kovaltsov GA, et al. 2020. *J. Geophys. Res. (Space Phys.)* 125:e27921

Usoskin IG, Kromer B, Ludlow F, et al. 2013. *Astron. Astrophys.* 552:L3

Valderrama J. 1886. *L'Astronomie* 5:388–89

van den Oord GHJ. 1990. *Astron. Astrophys.* 234:496–518

van Driel-Gesztelyi L, Green LM. 2015. *Liv. Rev. Solar Phys.* 12:1

Vaquero JM, Vázquez M, Sánchez Almeida J. 2017. *Solar Phys.* 292:33

Vesecky JF, Antiochos SK, Underwood JH. 1979. *Ap. J.* 233:987–97

Vida K, Leitzinger M, Kriskovics L, et al. 2019. *Astron. Astrophys.* 623:A49

Walkowicz LM, Basri G, Batalha N, et al. 2011. *Astron. J.* 141:50

Wang H, Ewell MW Jr., Zirin H, Ai G. 1994. *Ap. J.* 424:436–43

Warren HP, Brooks DH, Ugarte-Urra I, et al. 2018. *Ap. J.* 854:122

Wdowczyk J, Wolfendale AW. 1977. In *15th International Cosmic Ray Conference*, Vol. 5, pp. 270–73. Budapest, Hung.: Dept. of Cosmic Rays, Cent. Res. Inst. Phys. Hung. Acad. Sci.

Welsch BT. 2018. *Solar Phys.* 293:113

Wheatland MS. 2001. *Solar Phys.* 203:87–106

Wheatland MS. 2010. *Ap. J.* 710:1324–34

Wild JP, Smerd SF, Weiss AA. 1963. *Annu. Rev. Astron. Astrophys.* 1:291–366

Willson RC, Gulkis S, Janssen M, Hudson HS, Chapman GA. 1981. *Science* 211:700–2

Woods TN, Eparvier FG, Hock R, et al. 2012. *Solar Phys.* 275:115–43

Woods TN, Hock R, Eparvier F, et al. 2011. *Ap. J.* 739:59

Woods TN, Kopp G, Chamberlin PC. 2006. *J. Geophys. Res. (Space Phys.)* 111:A10S14

Yashiro S, Gopalswamy N, Akiyama S, Michalek G, Howard RA. 2005. *J. Geophys. Res. (Space Phys.)* 110:A12S05

Zwaan C. 1987. *Annu. Rev. Astron. Astrophys.* 25:83–111